A GENERALIZED FINITE ELEMENT BASED CRACK PATH PREDICTION FOR LINEAR ELASTIC FRACTURE MECHANICS

By

Omprakash Seresta

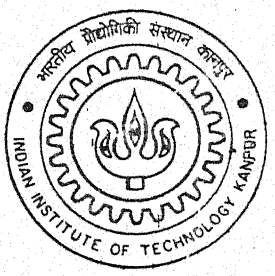

DEPARTMENT OF AEROSPACE ENGINEERING

Indian Institute of Technology Kanpur

FEBRUARY, 2002

A GENERALIZED FINITE ELEMENT BASED CRACK PATH PREDICTION FOR LINEAR ELASTIC FRACTURE MECHANICS

A Thesis Submitted
In Partial Fulfilment of the Requirements
for the Degree of
Master of Technology

by

OMPRAKASH SERESTA

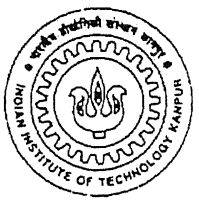

to the

DEPARTMENT OF AEROSPACE ENGINEERING
INDIAN INSTITUTE OF TECHNOLOGY KANPUR
INDIA

February, 2002

CERTIFICATE

It is certified that the work contained in the thesis entitled "***A Generalized Finite Element Based Crack Path Prediction For Linear Elastic Fracture Mechanics***", by ***Mr. Omprakash Seresta*** , has been carried out under our supervision and that this work has not been submitted elsewhere for a degree.

Dr. D. Yadav
Professor
Dept. of Aerospace Engineering and
I.I.T Kanpur

Dr. C.S. Upadhyay
Asst. Professor
Dept. of Aerospace Engineering
I.I.T. Kanpur

February, 2002

Acknowledgements

I express my sincere gratitude, regards and thanks to my supervisors Prof. C. S. Upadhyay and Prof. D. Yadav for their excellent guidance, invaluable suggestions and generous help at all the stages of my work. Their interest and confidence in me was the reason for all the success I have made.

I am extremely grateful to my friends Pradipta, Shamikc, Shamik and Arijit for all the encouragement and support I have received from them at all times. I am glad to record my thanks to my Structure Lab mates Amit, Mohite, Anil and others whose kindness and cooperation I remember with gratitude.

Once again, I would like to thank all my classmates for their smile and friendship making the life at I.I.T. Kanpur enjoyable and memorable.

Omprakash Seresta

Dedicated to My Parents and Teachers

Abstract

This thesis deals with the topic of generalized finite element method (GFEM) with particular reference to linear elastic fracture mechanics (LEFM). The presence of a crack in the domain leads to singular stresses at the crack tip, for linear elastic analysis. In this case, the conventional finite element analysis is known to lead to inferior quality crack parameters. The quality of extracted crack parameters can be improved only by significant mesh refinements at the crack tip. Use of refined meshes increases the computational load. In the present study, an effort has been made to characterise the crack parameters more accurately and (computationally) efficiently. The basic idea is to use specialized basis functions at the crack tip, using the asymptotic crack solutions. The method uses the partition of unity approach to make the approximation conforming. The code has been benchmarked with a large set of sample problems. Further, a crack propagation problem in planar elasticity is considered. Lastly, the problem of propagation of multiple, arbitrarily placed, cracks is considered.

Contents

List of Figures

List of Tables

Chapter 1

Introduction

1.1 Introduction

The generalized finite element method (GFEM) is a combination of classical finite element method (FEM) and partition of unity method (PUM). In generalized finite element (GFEM), the standard finite element spaces are augmented by adding special functions which reflect the known information about the boundary value problem and input data; e.g. the singular solution obtained from the local asymptotic expansion of the exact solution in the neighbourhood of a centre point, etc. The essential idea in this method is to add enrichment functions to the finite element approximation which contains a discontinuous displacement field. The method exploits the partition of unity property of finite elements which was noted by Melenk and Babuska [1], and Duarte and Oden [2], namely that the sum of the shape functions must be unity. The special functions are multiplied with the partition of unity to construct an augmented conforming finite element space. In this way the local approximability afforded by the special functions is included in the standard finite element approximation, while maintaining the existing infrastructure of finite element codes.

1.2 Literature survey

In the field of computational mechanics, extensive research has been done in the effective use of the finite element method for problems in fracture mechanics. Effort has been primarily focussed on the modification of the approximation, incorporating the singularity present in the domain. Of the various elements developed, collapsed quadrilateral elements and quarter point element requires special mention [16]. While direct application of standard elements is the most straightforward, a high degree of mesh refinement is required near the crack tip to capture the singular stress fields.

Recently, various methods that attempt to do away with the mesh have become popular for solving boundary value problems, for example, the element-free galerkin methods of Belytschko et al. [11]; the hp Clouds method of Duarte and Oden [2]. These methods in their purest form

get rid of the finite element method (FEM) completely, and intend to replace traditional finite element codes with a new infrastructure. The methods have had limited success because they have not successfully addressed the problem of the numerical integration of the entries of the discrete equations. For example, all meshless methods must still employ an integration mesh for the numerical integration. However, because the regions of integration which are often intersecting disks in two-dimensions (2D) or spheres in three-dimensions (3D) do not coincide with the integration mesh, it is very difficult to control the error of the numerical integration. Further, the various meshless methods also require special techniques for applying essential boundary conditions, e.g., the method of Lagrange multipliers which raise the issues of stability. An enriched element free galerkin method (EFG) was proposed by Fleming et al [4]. However, it has yielded good results only when adequate refinement (in the background mesh) is used near the crack tip. Moreover, the stresses computed also tend to be oscillatory near the crack tip unless substantial refinement is used. All these modern meshless methods are based implicitly or explicitly on using a partition of unity over the the domain to ensure continuity of the approximation. The partition of unity method (PUM) was developed by Babuska et al [1].
Recently, the generalized finite element method (GFEM) was proposed by Strouboulis et al [6] to do away with the problems encountered in common meshless methods. The Computational Mechanics Company (COMCO) is currently developing a new fast and robust solver for structural mechanics problem. It is based on a new solver technology, which promises to combine the modeling advantages and flexibility of finite element methods with the ease of use of meshless methods and with computational performance compatible or faster than modern finite element codes. The solver is based on proprietary extensions of meshless cloud methods and generalized finite element method (GFEM). It is being implemented in an hp-adaptive context within the computational environment PHLEX. Formally, the method is named generalized finite element partition of unity method or, for short, an element partition method (EPM) [7].
The present work, is a first step towards developing a generalized finite element based analysis platform for the study of quasi-static and dynamic crack propagation. The local asymptotic solution, at the crack tip, is chosen for enrichment. These special functions are made conforming by employing partition of unity based cut-off functions.

1.3 Thesis organization

The thesis is organised as follows:

1. In chapter 2, we briefly review the concepts of the re-entrant corner and its generalisation to linear elastic fracture mechanics. The procedure employed to calculate the different crack parameters are outlined in this chapter.

2. In chapter 3, a general procedure is implemented, based on energy principle, for deriving

the weak formulation studied in this work.

3. In chapter 4, we discuss the main features of the generalized finite element method employed in this work. An adaptive integration scheme tailored to the present work has been detailed elaborately.

4. In chapter 5, we present the numerical results obtained and a qualitative analysis has been done to compare the classical finite element solution and generalized finite element solution. Lastly an effort is made to predict the crack path using the above principle.

5. Finally in chapter 6, we summarize our work and draw the relevant conclusions and the scope for future work.

Chapter 2

Linear elastic fracture mechanics

2.1 Two dimensional planar elasticity

Equilibrium Equation

In planar elasticity problems, the variation of stress components in third direction is negligible. Also the body force part in fracture mechanics is absent, hence the equilibrium equations can be simplified as follows

$$\frac{\partial \sigma_{11}}{\partial x_1} + \frac{\partial \sigma_{12}}{\partial x_2} = 0 \tag{2.1}$$

$$\frac{\partial \sigma_{12}}{\partial x_1} + \frac{\partial \sigma_{22}}{\partial x_2} = 0 \tag{2.2}$$

Strain displacement relationship

If u_1 and u_2 are the two planar displacement components, then the strain-displacement relation is given by

$$\varepsilon_{11} = \frac{\partial u_1}{\partial x_1} \tag{2.3}$$

$$\varepsilon_{22} = \frac{\partial u_2}{\partial x_2} \tag{2.4}$$

$$\varepsilon_{12} = \frac{1}{2}\left(\frac{\partial u_1}{\partial x_2} + \frac{\partial u_2}{\partial x_1}\right) \tag{2.5}$$

The compatibility relation is given by

$$\frac{\partial^2 \varepsilon_{11}}{\partial x_2^2} + \frac{\partial^2 \varepsilon_{22}}{\partial x_1^2} - 2\frac{\partial^2 \varepsilon_{12}}{\partial x_1 \partial x_2} = 0 \tag{2.6}$$

Stress strain relationship

For the linear elasticity problem with isotropic materials, the stress strain relationship can be given as

$$\varepsilon_{11} = \frac{1}{E}[\sigma_{11} - \nu(\sigma_{22} + \sigma_{33})] \tag{2.7}$$

$$\varepsilon_{22} = \frac{1}{E}[\sigma_{22} - \nu(\sigma_{11} + \sigma_{33})] \tag{2.8}$$

$$\varepsilon_{33} = \frac{1}{E}[\sigma_{33} - \nu(\sigma_{11} + \sigma_{22})] \tag{2.9}$$

$$\varepsilon_{12} = \frac{(1+\nu)}{E}\sigma_{12} = \frac{1}{2G}\sigma_{12} \tag{2.10}$$

Plane deformation

For the case of plane stress i.e. for a very thin plate, the out of plane stresses are negligible in the interior points of the plate. Thus we have

$$\sigma_{13} = \sigma_{23} = \sigma_{33} = 0 \tag{2.11}$$

Thus the stress strain relation reduces to

$$\varepsilon_{11} = \frac{1}{E}[\sigma_{11} - \nu\sigma_{22}] \tag{2.12}$$

$$\varepsilon_{22} = \frac{1}{E}[\sigma_{22} - \nu\sigma_{11}] \tag{2.13}$$

$$\varepsilon_{12} = \frac{1}{2G}\sigma_{12} \tag{2.14}$$

Similarly for the plane strain case, i.e. for sufficiently thick plates , the through the thickness strain leads to

$$\varepsilon_{13} = \varepsilon_{23} = \varepsilon_{33} = 0 \tag{2.15}$$

$$\sigma_{33} = \nu(\sigma_{11} + \sigma_{22}) \tag{2.16}$$

Thus the stress strain relation reduces to

$$\varepsilon_{11} = \frac{(1-\nu^2)}{E}[\sigma_{11} - \frac{\nu}{(1-\nu)}\sigma_{22}] \tag{2.17}$$

$$\varepsilon_{22} = \frac{(1-\nu^2)}{E}[\sigma_{22} - \frac{\nu}{(1-\nu)}\sigma_{11}] \tag{2.18}$$

$$\varepsilon_{12} = \frac{(1-\nu^2)}{2G}[1 + \frac{\nu}{(1-\nu)}]\sigma_{12} \tag{2.19}$$

or, a general representation for the planar constitutive relationship can be given by

$$\varepsilon_{11} = \frac{1}{E^*}[\sigma_{11} - \nu^*\sigma_{22}] \tag{2.20}$$

$$\varepsilon_{22} = \frac{1}{E^*}[\sigma_{22} - \nu^*\sigma_{11}] \tag{2.21}$$

$$\varepsilon_{12} = \frac{1+\nu^*}{E^*}\sigma_{12} \tag{2.22}$$

where

$$E^* = \begin{cases} E \text{ for plane stress} \\ \frac{E}{1-\nu^2} \text{ for plane strain} \end{cases} \tag{2.23}$$

$$\nu^* = \begin{cases} \nu \text{ for planestress} \\ \frac{\nu}{1-\nu} \text{ for planestrain} \end{cases} \tag{2.24}$$

2.2 Linear elastic fracture mechanics

Below, a brief outline of the theory of fracture mechanics for linear, plane elasticity, is given Consider a vertex A, as shown in figure (2.1). In the case of planar elasticity, the *Airy stress*

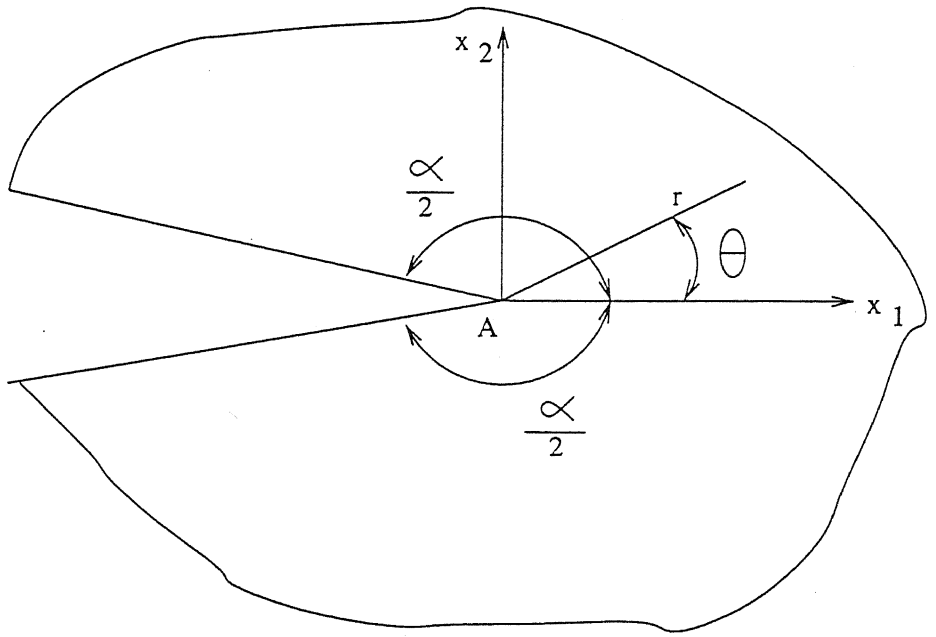

Figure 2.1: An arbitrary domain with a re entrant corner. The local cartesian and polar coordinate system with respect to the vertex A

function U satisfies the biharmonic equation :

$$\left(\frac{\partial^2}{\partial r^2} + \frac{1}{r}\frac{\partial}{\partial r} + \frac{1}{r^2}\frac{\partial^2}{\partial \theta^2}\right)\left(\frac{\partial^2}{\partial r^2} + \frac{1}{r}\frac{\partial}{\partial r} + \frac{1}{r^2}\frac{\partial^2}{\partial \theta^2}\right)U = 0 \tag{2.25}$$

Let us consider solutions of the form (see [12]) :

$$U = U(r,\theta) = r^{\lambda+1}F(\theta) \tag{2.26}$$

Therefore , $F(\theta)$ must satisfy :

$$F'''' + 2(\lambda^2+1)F'' + (\lambda^2-1)F = 0 \tag{2.27}$$

where the prime represent differentiation with respect to θ. The general solution of equation (2.27) for $\lambda \neq 0$ and $\lambda \neq \pm 1$ is :

$$F(\theta) = a_1\cos(\lambda-1)\theta + a_2\cos(\lambda+1)\theta + a_3\sin(\lambda-1)\theta + a_4\sin(\lambda+1)\theta \tag{2.28}$$

The modifications necessary for the cases $\lambda = 0$ and $\lambda = \pm 1$ are obvious. The stress components are related to the stress function U as follows :

$$\sigma_r = \frac{1}{r}\frac{\partial U}{\partial r} + \frac{1}{r^2}\frac{\partial^2 U}{\partial \theta^2} = r^{\lambda-1}[(\lambda+1)F(\theta) + F''(\theta)] \tag{2.29}$$

$$\sigma_\theta = \frac{\partial^2 U}{\partial r^2} = \lambda(\lambda+1)r^{\lambda-1}F(\theta) \tag{2.30}$$

$$\tau_{r\theta} = -\frac{1}{r}\frac{\partial^2 U}{\partial r \partial \theta} + \frac{1}{r^2}\frac{\partial U}{\partial \theta} = -\lambda r^{\lambda-1}F'(\theta) \tag{2.31}$$

Let us assume that the edges at $\theta = \pm\frac{\alpha}{2}$ are stress free which implies that : $\sigma_\theta = \tau_{r\theta} = 0$ on these edges. Consequently, from equation (2.28), (2.31) and (2.31), after straightforward algebraic manipulation, we have

$$\begin{bmatrix} \cos(\lambda-1)\frac{\alpha}{2} & \cos(\lambda+1)\frac{\alpha}{2} & 0 & 0 \\ \Lambda\sin(\lambda-1)\frac{\alpha}{2} & \sin(\lambda+1)\frac{\alpha}{2} & 0 & 0 \\ 0 & 0 & \sin(\lambda-1)\frac{\alpha}{2} & \sin(\lambda+1)\frac{\alpha}{2} \\ 0 & 0 & \Lambda\cos(\lambda-1)\frac{\alpha}{2} & \cos(\lambda+1)\frac{\alpha}{2} \end{bmatrix} \begin{Bmatrix} a_1 \\ a_2 \\ a_3 \\ a_4 \end{Bmatrix} = 0 \tag{2.32}$$

where Λ is defined as

$$\Lambda = \frac{\lambda-1}{\lambda+1} \tag{2.33}$$

This gives rise to two sets of decoupled simultaneous equations in terms of a_1, a_2 and a_3, a_4. A non trivial solution exists only if the corresponding determinant vanishes. This is possible if either

$$\cos(\lambda-1)\frac{\alpha}{2}\sin(\lambda+1)\frac{\alpha}{2} - \Lambda\sin(\lambda-1)\frac{\alpha}{2}\cos(\lambda+1)\frac{\alpha}{2} = 0 \tag{2.34}$$

or

$$\sin(\lambda-1)\frac{\alpha}{2}\cos(\lambda+1)\frac{\alpha}{2} - \Lambda\cos(\lambda-1)\frac{\alpha}{2}\sin(\lambda+1)\frac{\alpha}{2} = 0 \tag{2.35}$$

To find non trivial solution for equation (2.32) we set $a_3 = a_4 = 0$ and find λ such that equation (2.34) satisfied, or we set $a_1 = a_2 = 0$ and find λ such that equation (2.35) is satisfied. Equations (2.34) and (2.35) can be simplified to

$$\sin\lambda\alpha + \lambda\sin\alpha = 0 \tag{2.36}$$

$$\sin\lambda\alpha - \lambda\sin\alpha = 0 \tag{2.37}$$

Now λ can be complex and either a simple or multiple root of equation (2.36) or equation (2.37) If λ is complex, then its conjugate is also a root of equation (2.36) or equation (2.37) , and both the real and the imaginary parts of $r^{\lambda+1}F(\theta)$ are solutions of equation (2.25). If λ is a solution, then $-\lambda$ is also a solution; however the corresponding stress field has finite strain energy only if the real part of λ is greater than zero.

Assume that $\lambda_i^{(1)}$ (i=1,2....) is a solution of equation (2.36) and $\lambda_i^{(1)}$ is real and simple. Then from equation (2.32) :

$$a_1 \cos(\lambda_i^{(1)} - 1)\frac{\alpha}{2} + a_2 \cos(\lambda_i^{(1)} + 1)\frac{\alpha}{2} = 0 \tag{2.38}$$

$$a_1 \Lambda_i^{(1)} \sin(\lambda_i^{(1)} - 1)\frac{\alpha}{2} + a_2 \sin(\lambda_i^{(1)} + 1)\frac{\alpha}{2} = 0 \tag{2.39}$$

Let us define :

$$Q_i^{(1)} = -\frac{\cos(\lambda_i^{(1)} - 1)\frac{\alpha}{2}}{\cos(\lambda_i^{(1)} + 1)\frac{\alpha}{2}} = -\frac{\Lambda_i^{(1)} \sin(\lambda_i^{(1)} - 1)\frac{\alpha}{2}}{\sin(\lambda_i^{(1)} + 1)\frac{\alpha}{2}} \tag{2.40}$$

With this notation, equation (2.26) can be written as :

$$U = r^{\lambda_i^{(1)}+1}(\cos(\lambda_i^{(1)} - 1)\theta + Q_i^{(1)} \cos(\lambda_i^{(1)} + 1)\theta) \tag{2.41}$$

Similarly, if $\lambda_i^{(2)}$ is a real, simple root of equation (2.37), then the stress function is :

$$U = r^{\lambda_i^{(2)}+1}(\sin(\lambda_i^{(1)} - 1)\theta + Q_i^{(2)} \sin(\lambda_i^{(2)} + 1)\theta) \tag{2.42}$$

where $Q_i^{(2)}$ is defined as :

$$Q_i^{(2)} = -\frac{\sin(\lambda_i^{(2)} - 1)\frac{\alpha}{2}}{\sin(\lambda_i^{(2)} + 1)\frac{\alpha}{2}} = -\frac{\lambda_i^{(2)} - 1}{\lambda_i^{(2)} + 1}\frac{\cos(\lambda_i^{(2)} - 1)\frac{\alpha}{2}}{\cos(\lambda_i^{(2)} + 1)\frac{\alpha}{2}} \tag{2.43}$$

Equation (2.41) is symmetric with respect to θ and equation (2.42) is anti symmetric with respect to θ. From equation (2.41) and equation (2.42), expressions for stress and strain can be derived. The stress and displacement field corresponding to equation (2.41) are called *Mode I* fields which are given by :

$$u_{1i}^{(1)} = \frac{1}{2G} r^{\lambda_i^{(1)}} [(\kappa - Q_i^{(1)}(\lambda_i(1) + 1)) \cos \lambda_i^{(1)}\theta - \lambda_i^{(1)} \cos(\lambda_i^{(1)} - 2)\theta] \tag{2.44}$$

$$u_{2i}^{(1)} = \frac{1}{2G} r^{\lambda_i^{(1)}} [(\kappa + Q_i^{(1)}(\lambda_i(1) + 1)) \sin \lambda_i^{(1)}\theta + \lambda_i^{(1)} \sin(\lambda_i^{(1)} - 2)\theta] \tag{2.45}$$

which can be written as

$$\mathbf{u}_i^{(1)} \equiv \left\{ \begin{array}{c} u_{1i}^{(1)} \\ u_{2i}^{(1)} \end{array} \right\} = \frac{1}{2G} r^{\lambda_i^{(1)}} \{\Psi_i^{(1)}(\theta)\} \tag{2.46}$$

where κ is Kolosov's constant given by :

$$\kappa = 3 - 4\nu \text{ for plane strain} \tag{2.47}$$

$$\kappa = \frac{3 - \nu}{1 + \nu} \text{ for plane stress} \tag{2.48}$$

The *Mode I* stress tensor components are :

$$\sigma_{11i}^{(1)} = \lambda_i^{(1)} r^{\lambda_i^{(1)}-1}[2 - Q_i^{(1)}(\lambda_i^{(1)} + 1) \cos(\lambda_i^{(1)} - 1)\theta - (\lambda_i^{(1)} - 1) \cos(\lambda_i^{(1)} - 3)\theta] \tag{2.49}$$

$$\sigma_{22i}^{(1)} = \lambda_i^{(1)} r^{\lambda_i^{(1)}-1}[2 + Q_i^{(1)}(\lambda_i^{(1)} + 1) \cos(\lambda_i^{(1)} - 1)\theta + (\lambda_i^{(1)} - 1) \cos(\lambda_i^{(1)} - 3)\theta] \tag{2.50}$$

$$\sigma_{12i}^{(1)} = \lambda_i^{(1)} r^{\lambda_i^{(1)}-1}[(\lambda_i^{(1)} - 1) \sin(\lambda_i^{(1)} - 3)\theta + Q_i^{(1)}(\lambda_i^{(1)} + 1) \sin(\lambda_i^{(1)} - 1)\theta] \tag{2.51}$$

The stress and displacement fields corresponding to equation (2.42) are called *Mode II* fields which are given by :

$$u_{1i}^{(2)} = \frac{1}{2G} r^{\lambda_i^{(2)}} [(\kappa - Q_i^{(2)}(\lambda_i(2)+1)) \sin \lambda_i^{(2)}\theta - \lambda_i^{(2)} \sin(\lambda_i^{(2)} - 2)\theta] \quad (2.52)$$

$$u_{2i}^{(2)} = \frac{1}{2G} r^{\lambda_i^{(2)}} [(\kappa + Q_i^{(2)}(\lambda_i(2)+1)) \cos \lambda_i^{(2)}\theta + \lambda_i^{(2)} \cos(\lambda_i^{(2)} - 2)\theta] \quad (2.53)$$

which can be written as

$$\mathbf{u}_i^{(2)} \equiv \left\{ \begin{array}{c} u_{1i}^{(2)} \\ u_{2i}^{(2)} \end{array} \right\} = \frac{1}{2G} r^{\lambda_i^{(2)}} \{\Psi_i^{(2)}(\theta)\} \quad (2.54)$$

The *Mode II* stress tensor components are :

$$\sigma_{11i}^{(2)} = \lambda_i^{(2)} r^{\lambda_i^{(2)}-1} [2 - Q_i^{(2)}(\lambda_i^{(2)}+1) \sin(\lambda_i^{(2)} - 1)\theta - (\lambda_i^{(2)} - 1) \sin(\lambda_i^{(2)} - 3)\theta] \quad (2.55)$$

$$\sigma_{22i}^{(2)} = \lambda_i^{(2)} r^{\lambda_i^{(2)}-1} [2 + Q_i^{(2)}(\lambda_i^{(2)}+1) \sin(\lambda_i^{(2)} - 1)\theta + (\lambda_i^{(2)} - 1) \sin(\lambda_i^{(2)} - 3)\theta] \quad (2.56)$$

$$\sigma_{12i}^{(2)} = -\lambda_i^{(2)} r^{\lambda_i^{(2)}-1} [(\lambda_i^{(2)} - 1) \cos(\lambda_i^{(2)} - 3)\theta + Q_i^{(2)}(\lambda_i^{(2)}+1) \cos(\lambda_i^{(2)} - 1)\theta] \quad (2.57)$$

Thus in the general case in the vicinity of the re-entrant corner, the solution can be written using equation (2.46) and (2.54) as :

$$\{\mathbf{u}\} = \sum_{i=1}^{\infty} \frac{A_i^{(1)}}{2G} r^{\lambda_i^{(1)}} \{\Psi_i^{(1)}(\theta)\} + \sum_{i=1}^{\infty} \frac{A_i^{(2)}}{2G} r^{\lambda_i^{(2)}} \{\Psi_i^{(2)}(\theta)\} \quad (2.58)$$

The coefficients $A_i^{(1)}$ and $A_i^{(2)}$ are called generalized stress intensity factors. In case of a crack we have $\alpha = 2\pi$. Equations (2.36) and (2.37) are identical ($\sin 2\pi\lambda = 0$), and all roots are real and simple :

$$\lambda_i^{(1)} = \lambda_i^{(2)} = \pm\frac{1}{2}, \ \pm\frac{3}{2}, \ \pm 2, \ \pm\frac{5}{2} \quad (2.59)$$

The coefficients $A_i^{(1)}$ and $A_i^{(2)}$ are related to *Mode I* and *Mode II* stress intensity factors of linear elastic fracture mechanics. In linear elastic fracture mechanics three modes of crack opening are present in three dimension. In plane elasticity, only first two modes are present. These are :

1. Mode I - Tensile Mode or Opening Mode
2. Mode II - Shear Mode or Sliding Mode

Below, we give the expression for the displacements and stresses for the mentioned two modes.

Mode I

For Mode I type of loading the solution in the vicinity of the crack tip is given by

$$\sigma_{11} = \frac{K_I}{\sqrt{2\pi r}} \cos\frac{\theta}{2}[1 - \sin\frac{\theta}{2}\sin\frac{3\theta}{2}] \quad (2.60)$$

$$\sigma_{22} = \frac{K_I}{\sqrt{2\pi r}} \cos\frac{\theta}{2}[1 + \sin\frac{\theta}{2}\sin\frac{3\theta}{2}] \quad (2.61)$$

$$\sigma_{12} = \frac{K_I}{\sqrt{2\pi r}} \cos\frac{\theta}{2}\sin\frac{\theta}{2}\cos\frac{3\theta}{2} \quad (2.62)$$

where K_I is the stress intensity factor in *Mode I*. The displacement components u_1 and u_2 are given as follows

$$u_1 = \frac{K_I}{G}\left(\frac{r}{2\pi}\right)^{\frac{1}{2}} \cos\frac{\theta}{2}\left[1 - 2\nu + \sin^2\frac{\theta}{2}\right] \tag{2.63}$$

$$u_2 = \frac{K_I}{G}\left(\frac{r}{2\pi}\right)^{\frac{1}{2}} \sin\frac{\theta}{2}\left[2 - 2\nu + \cos^2\frac{\theta}{2}\right] \tag{2.64}$$

$$\sigma_{33} = 0 \text{ for plane stress}$$

$$\sigma_{33} = \nu(\sigma_{11} + \sigma_{22}) \text{ for plane strain}$$

Mode II

For mode II type of loading the solution in the vicinity of crack tip is given by

$$\sigma_{11} = -\frac{K_{II}}{\sqrt{2\pi r}} \sin\frac{\theta}{2}[2 + \cos\frac{\theta}{2}\cos\frac{3\theta}{2}] \tag{2.65}$$

$$\sigma_{22} = \frac{K_{II}}{\sqrt{2\pi r}} \sin\frac{\theta}{2}\cos\frac{\theta}{2}\cos\frac{3\theta}{2} \tag{2.66}$$

$$\sigma_{12} = \frac{K_{II}}{\sqrt{2\pi r}} \cos\frac{\theta}{2}[1 - \sin\frac{\theta}{2}\sin\frac{3\theta}{2}] \tag{2.67}$$

where K_{II} is the stress intensity factor in *Mode II*. The displacement components u_1 and u_2 are given as follows

$$u_1 = \frac{K_{II}}{G}\left(\frac{r}{2\pi}\right)^{\frac{1}{2}} \sin\frac{\theta}{2}\left[2 - 2\nu + \cos^2\frac{\theta}{2}\right] \tag{2.68}$$

$$u_2 = \frac{K_{II}}{G}\left(\frac{r}{2\pi}\right)^{\frac{1}{2}} \cos\frac{\theta}{2}\left[-1 + 2\nu + \sin^2\frac{\theta}{2}\right] \tag{2.69}$$

As it is evident from the functional form of σ_{ij} that singularities in the form of $r^{-1/2}$ are present. This means that when $r \to 0$, σ_{11} and σ_{22} becomes infinite.

Mixed mode analysis

The near tip displacement fields for combined *Mode I* and *Mode II* loading are obtained by superimposing the two fields and is given by :

$$u_1 = \frac{K_I}{2G}\left(\frac{r}{2\pi}\right)^{\frac{1}{2}} \cos\frac{\theta}{2}[\kappa - 1 + 2\sin^2\frac{\theta}{2}] + \frac{K_{II}}{2G}\left(\frac{r}{2\pi}\right)^{\frac{1}{2}} \sin\frac{\theta}{2}[\kappa + 1 + 2\cos^2\frac{\theta}{2}] \tag{2.70}$$

$$u_2 = \frac{K_I}{2G}\left(\frac{r}{2\pi}\right)^{\frac{1}{2}} \sin\frac{\theta}{2}[\kappa + 1 - 2\cos^2\frac{\theta}{2}] - \frac{K_{II}}{2G}\left(\frac{r}{2\pi}\right)^{\frac{1}{2}} \cos\frac{\theta}{2}[\kappa - 1 - 2\sin^2\frac{\theta}{2}] \tag{2.71}$$

Similarly, the stress field is given by :

$$\begin{Bmatrix} \sigma_{11} \\ \sigma_{22} \\ \sigma_{12} \end{Bmatrix} = \frac{K_I}{\sqrt{2\pi r}} \begin{Bmatrix} \cos\frac{\theta}{2}\left(1 - \sin\frac{\theta}{2}\sin\frac{3\theta}{2}\right) \\ \cos\frac{\theta}{2}\left(1 + \sin\frac{\theta}{2}\sin\frac{3\theta}{2}\right) \\ \cos\frac{\theta}{2}\sin\frac{\theta}{2}\cos\frac{3\theta}{2} \end{Bmatrix} + \frac{K_{II}}{\sqrt{2\pi r}} \begin{Bmatrix} -\sin\frac{\theta}{2}\left(2 + \cos\frac{\theta}{2}\cos\frac{3\theta}{2}\right) \\ \sin\frac{\theta}{2}\cos\frac{\theta}{2}\cos\frac{3\theta}{2} \\ \cos\frac{\theta}{2}\left(1 - \sin\frac{\theta}{2}\sin\frac{3\theta}{2}\right) \end{Bmatrix} \tag{2.72}$$

The above general definition of the asymptotic solution near the crack tip is fundamental to the process of quasi static crack propagation. Below, we define the J integral that is used to characterise the criticallity of an existing crack.

2.2.1 J integral

Taken along a material curve Γ which is traversed in the counter clockwise direction between the two crack sides , the J integral is defined as

$$J = \int_{\Gamma} (W dx_2 - T_i \frac{\partial u_i}{\partial x_1} ds) \tag{2.73}$$

where $W = \int_0^{\varepsilon_{ij}} \sigma_{ij} d\varepsilon_{ij}$ is the deformation energy per unit volume, s is the arc length and T_i is the traction exerted on the body bounded by the curve Γ and crack surface.

$$T_i = \sigma_{ij} n_j$$

where n_j is the unit outward normal to the curve Γ. Two important characteristics of J integral

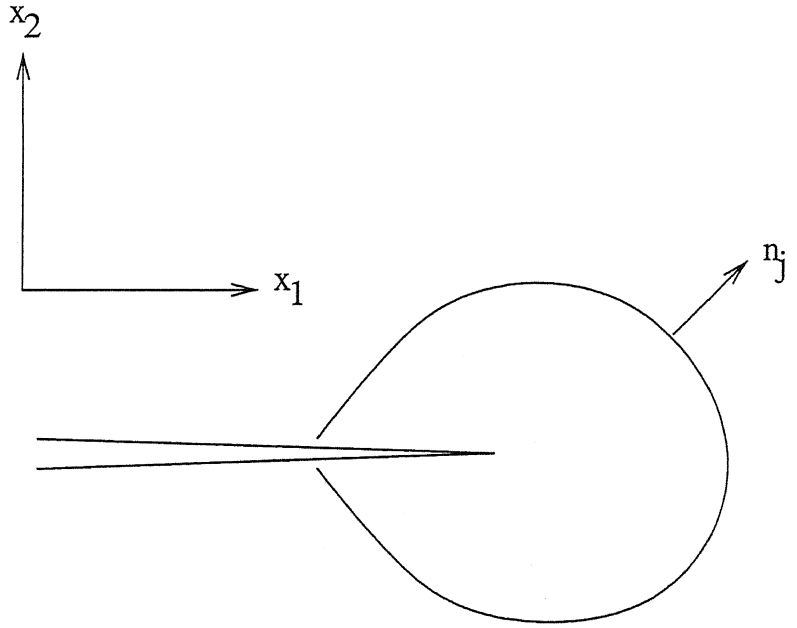

Figure 2.2: Computation of J integral

are

- It is path independent for linearly elastic bodies.
- For linearly elastic bodies, J integral represents the energy release rate and is same as the energy release rate G, proposed by Griffith [15].

It can be shown for Mode I loading condition

$$J = \frac{K_I^2}{E^*}$$

and for Mode II loading condition

$$J = \frac{K_{II}^2}{E^*}$$

Thus for mixed mode analysis,

$$J = \frac{{K_I}^2}{E^*} + \frac{K_{II}^2}{E^*} \tag{2.74}$$

Thus we note that the computation of the stress intensity factors is essential for obtaining the J integral

Computation of stress intensity factors

The stress intensity factor can be computed by several methods. Below we consider one of the method outlined in [3], which employ contour form of the interaction integral. The local coordinates are the crack tip coordinates with the x_1 axis parallel to the crack faces (see figure 2.2). Two states of cracked body are considered following [3]. State 1 $(\sigma_{ij}^1, \varepsilon_{ij}^1, u_i^1)$ corresponds to the actual state and state 2 $(\sigma_{ij}^2, \varepsilon_{ij}^2, u_i^2)$ is an auxiliary state which will be chosen as the asymptotic field for *Mode I* and *Mode II*. The J integral for the sum of the two states is

$$J^{(1+2)} = \int_\Gamma \Big[\frac{1}{2}(\sigma_{ij}^1 + \sigma_{ij}^2)(\varepsilon_{ij}^1 + \varepsilon_{ij}^2)\delta_{1j} - (\sigma_{ij}^1 + \sigma_{ij}^2)\frac{\partial(u_i^1 + u_i^2)}{\partial x_1}\Big] n_j d\Gamma \tag{2.75}$$

Expanding and rearranging the terms give

$$J^{(1+2)} = J^{(1)} + J^{(2)} + I^{(1,2)} \tag{2.76}$$

where $I^{(1,2)}$ is the interaction integral for states 1 and 2,

$$I^{(1,2)} = \int_\Gamma \Big[W^{(1,2)}\delta_{1,j} - \sigma_{ij}^{(1)}\frac{\partial u_i^2}{\partial x_1} - \sigma_{ij}^{(2)}\frac{\partial u_i^1}{\partial x_1}\Big] n_j d\Gamma \tag{2.77}$$

and $W^{(1,2)}$ is the interaction energy, given by

$$W^{(1,2)} = \sigma_{ij}^{(1)}\varepsilon_{ij}^{(2)} = \sigma_{ij}^{(2)}\varepsilon_{ij}^{(1)} \tag{2.78}$$

Substituting equation (2.74) for the combined states and rearranging the term gives

$$J^{(1+2)} = J^{(1)} + J^{(2)} + \frac{2}{E^*}(K_I^{(1)}K_I^{(2)} + K_{II}^{(1)}K_{II}^{(2)}) \tag{2.79}$$

Equating equation (2.76) and (2.79) leads to the following eqaution :

$$I^{(1,2)} = \frac{2}{E^*}(K_I^{(1)}K_I^{(2)} + K_{II}^{(1)}K_{II}^{(2)}) \tag{2.80}$$

Now choosing state 2 as $Mode\ \ I$ asymptotic field with $K_I^{(2)} = 1$ and $K_{II}^{(2)} = 0$ gives $Mode\ \ I$ stress intensity factor for state 1 or actual state in terms of interaction integral as

$$K_I^{(1)} = \frac{E^*}{2} I^{(1,Mode\ \ I)} \tag{2.81}$$

Then choosing the auxillary state as that for $Mode\ \ II$ asymptotic field with $K_I^{(2)} = 0$ and $K_{II}^{(2)} = 1$ gives $Mode\ \ II$ stress intensity factor for state 1 in terms of interaction integral as

$$K_{II}^{(1)} = \frac{E^*}{2} I^{(1,Mode\ \ II)} \tag{2.82}$$

2.2.2 Crack growth criteria

We briefly review the crack growth law used to specify the direction of crack growth. The criteria for determining the crack growth direction can be summed up in the following three categories :

1. The maximum energy release rate criterion
2. The maximum tangential stress criterion
3. The minimum strain energy criterion

In the present work, we used the maximum tangential stress criterion or the maximum circumferential (hoop) stress criterion, which is identical to maximum energy release rate criterion for linear elastic fracture mechanics. The maximum tangential stress criterion states that the crack will propagate from its tip in a direction θ_c so that the circumferential stress $\sigma_{\theta\theta}$ is maximum. Therefore, the critical angle θ_c defining the radial direction of propagation can be determined by setting the shear stresses associated to zero because this corresponds to the principal direction. Thus

$$\sigma_{r\theta} = \frac{1}{2\pi r} \cos\frac{\theta}{2}\Big[\frac{1}{2} K_I \sin\theta + \frac{1}{2} K_{II}(3\cos\theta - 1)\Big] = 0 \tag{2.83}$$

This leads to the equation defining the angle of crack propagation (in the tip coordinate system) θ_c

$$K_I \sin\theta_c + K_{II}(3\cos\theta_c - 1) = 0 \tag{2.84}$$

Solving the above equation gives

$$\theta_c = 2\arctan\frac{1}{4}\Big(\frac{K_I}{K_{II}} \pm \sqrt{(\frac{K_I}{K_{II}})^2 + 8}\Big) \tag{2.85}$$

For $K_{II} = 0$, $\theta_c = 0$, i.e. the crack propagates straight, without turning.

Chapter 3

Finite element formulation

3.1 Finite element formulation using energy principle

The total potential for the plate is given by

$$\Pi\left(\mathbf{u}\right) = \sum_{e=1}^{N} \pi^{e}\left(\mathbf{u}\right), \tag{3.1}$$

where π^e is the total potential of the non-intersecting (but adjacent) sub-domains e which are part of the domain (N sub-domains are considered here). The total potential can be expressed in terms of internal strain energy $U^{(e)}$ and external work done $W^{(e)}$, as follows:

$$\pi^{e}\left(\mathbf{u}\right) = U^{(e)} - W^{(e)}. \tag{3.2}$$

$$\Pi(\mathbf{u}) = \frac{1}{2}\int\{\sigma_{xx}(\mathbf{u})\varepsilon_{xx}(\mathbf{u})+\sigma_{xy}(\mathbf{u})\gamma_{xy}(\mathbf{u})+\sigma_{yy}(\mathbf{u})\varepsilon_{yy}(\mathbf{u})\}dA-\int_{A}(f_x u+f_y v)dA-\int_{\Gamma}(T_x u+T_y v)ds \tag{3.3}$$

where $\{\mathbf{f}\}$ is the body force vector, $\{\mathbf{T}\}$ is the traction vector and $\{\mathbf{u}\}$ is the displacement vector given by :

$$\{\mathbf{f}\} = \begin{Bmatrix} f_x \\ f_y \end{Bmatrix}$$

$$\{\mathbf{T}\} = \begin{Bmatrix} T_x \\ T_y \end{Bmatrix}$$

$$\{\mathbf{u}\} = \begin{Bmatrix} u \\ v \end{Bmatrix}$$

Minimizing the total potential energy gives

$$\delta^{(1)}(\Pi(\mathbf{u})) = lim_{\alpha\to 0}\frac{\Pi(\mathbf{u}+\alpha\mathbf{w})-\Pi(\mathbf{u})}{\alpha} = 0$$

where $\{\mathbf{w}\}$ is the perturbation vector

$$\{\mathbf{w}\} = \begin{Bmatrix} w_x \\ w_y \end{Bmatrix}$$

$$\delta^{(1)}(\Pi(\mathbf{u})) = \int_A (\sigma_{xx}(\mathbf{u})\varepsilon_{xx}(\mathbf{w}) + \sigma_{xy}(\mathbf{u})\gamma(\mathbf{w}) + \sigma_{yy}(\mathbf{u})\varepsilon_{yy}(\mathbf{w})) - \int_A (f_x w_x + f_y w_y)dA - \int_\Gamma (T_x w_x + T_y w_y)ds$$

Hence the bilinear form can be written as :

$$\beta(\mathbf{u},\mathbf{w}) = \int_A (\sigma_{xx}(\mathbf{u})\varepsilon_{xx}(\mathbf{w}) + \sigma_{xy}(\mathbf{u})\gamma_{xy}(\mathbf{w}) + \sigma_{yy}(\mathbf{u})\varepsilon_{yy}(\mathbf{w}))dA \tag{3.4}$$

$$F(\mathbf{w}) = \int_A (f_x w_x + f_y w_y)dA + \int_\Gamma (T_x w_x + T_y w_y)ds \tag{3.5}$$

3.2 Finite element approximation

$$\{\mathbf{u}_{FEM}\} = \begin{Bmatrix} \sum_{i=1}^{n} u_i \Phi_i(x,y) \\ \sum_{i=1}^{n} v_i \Phi_i(x,y) \end{Bmatrix}$$

$$\{\mathbf{u}_{FEM}\} = \begin{bmatrix} \Phi_1 & 0 & \Phi_2 & 0 & \Phi_3 & 0 & .. & .. \\ 0 & \Phi_1 & 0 & \Phi_2 & 0 & \Phi_3 & .. & .. \end{bmatrix} \begin{Bmatrix} u_1 \\ v_1 \\ u_2 \\ v_2 \\ u_3 \\ v_3 \\ . \\ . \end{Bmatrix}$$

$$\{\mathbf{u}_{FEM}\} = [\Phi]\{\mathbf{U}\}$$

Similarly,

$$\{\mathbf{w}\} = \begin{Bmatrix} \sum_{i=1}^{n} w_{xi} \Phi_i \\ \sum_{i=1}^{n} w_{yi} \Phi_i \end{Bmatrix}$$

$$\{\mathbf{w}\} = [\Phi]\{\mathbf{W}\}$$

Triangular elements are used in the finite element approximation employed in this study, along with hierarchic shape functions of order p ($p \leq 3$). n is the number of degrees of freedom for each element and it is equal to $\frac{(p+1)(p+2)}{2}$ for triangular elements. Φ_i are shape functions in global coordinate system x and y.

Let the stress and strain vectors corresponding to $\{\mathbf{u}\}$ be $\{\boldsymbol{\sigma}\}$ and $\{\boldsymbol{\varepsilon}\}$ which can be defined as:

$$\{\boldsymbol{\sigma}\} = \begin{Bmatrix} \sigma_x \\ \sigma_y \\ \sigma_{xy} \end{Bmatrix} \qquad \{\boldsymbol{\varepsilon}\} = \begin{Bmatrix} \varepsilon_x \\ \varepsilon_y \\ \gamma_{xy} \end{Bmatrix} \tag{3.6}$$

From the generalized Hooke's law which relates stress components to the respective strain components in global coordinate system, we have

$$[\boldsymbol{\sigma}] = [\bar{\mathbf{Q}}]\{\boldsymbol{\varepsilon}\} \tag{3.7}$$

where the material stiffness matrix $[\bar{\mathbf{Q}}]$ is given by :

$$[\bar{\mathbf{Q}}] = \begin{bmatrix} \frac{E}{1-\nu^2} & \frac{\nu E}{1-\nu^2} & 0 \\ \frac{\nu E}{1-\nu^2} & \frac{E}{1-\nu^2} & 0 \\ 0 & 0 & G \end{bmatrix} \text{ for plane stress} \tag{3.8}$$

$$[\bar{\mathbf{Q}}] = \begin{bmatrix} \frac{E(1-\nu)}{1-\nu-2\nu^2} & \frac{\nu E}{1-\nu-2\nu^2} & 0 \\ \frac{\nu E}{1-\nu-2\nu^2} & \frac{E(1-\nu)}{1-\nu-2\nu^2} & 0 \\ 0 & 0 & G \end{bmatrix} \text{ for plane strain} \tag{3.9}$$

The strain can be represented as:

$$\{\varepsilon\} = [\bar{\mathbf{D}}]\{\mathbf{u}\} \tag{3.10}$$

where $[\bar{\mathbf{D}}]$ is a differential operator in terms of global coordinates such that

$$[\bar{\mathbf{D}}] = \begin{bmatrix} \frac{\partial}{\partial x} & 0 \\ 0 & \frac{\partial}{\partial y} \\ \frac{\partial}{\partial y} & \frac{\partial}{\partial x} \end{bmatrix} \tag{3.11}$$

Hence, the strain field using finite element approximation is given by :

$$\{\varepsilon(\mathbf{u}_{FEM})\} = [\bar{\mathbf{D}}]\{\mathbf{u}_{FEM}\} \tag{3.12}$$

Substituting the expression for $\mathbf{u}_{FEM}$, we have

$$\{\varepsilon(\mathbf{u}_{FEM})\} = [\mathbf{B}]\{\mathbf{U}\} \tag{3.13}$$

where $[\mathbf{B}]$ is given as :

$$[\mathbf{B}] = \begin{bmatrix} \frac{\partial\Phi_1}{\partial x} & 0 & \frac{\partial\Phi_2}{\partial x} & 0 & \frac{\partial\Phi_3}{\partial x} & 0 & .. & .. \\ 0 & \frac{\partial\Phi_1}{\partial y} & 0 & \frac{\partial\Phi_2}{\partial y} & 0 & \frac{\partial\Phi_3}{\partial y} & .. & .. \\ \frac{\partial\Phi_1}{\partial y} & \frac{\partial\Phi_1}{\partial x} & \frac{\partial\Phi_2}{\partial y} & \frac{\partial\Phi_2}{\partial x} & \frac{\partial\Phi_3}{\partial y} & \frac{\partial\Phi_3}{\partial x} & .. & .. \end{bmatrix} \tag{3.14}$$

Similarly, for

$$\varepsilon(\mathbf{w}) = [\mathbf{B}]\{\mathbf{W}\}$$

Thus, in finite element approximation the bilinear form can be written as :

$$\begin{aligned} \beta(\mathbf{u}_{FEM}, \mathbf{w}) &= \int_A \{\varepsilon^T(\mathbf{w})\}\{\sigma(\mathbf{u}_{FEM})\}dA \\ \beta(\mathbf{u}_{FEM}, \mathbf{w}) &= [\mathbf{B}]\{\mathbf{W}\})^T[\bar{\mathbf{D}}]([\mathbf{B}]\{\mathbf{U}\} \end{aligned}$$

$$\beta(\mathbf{u}_{FEM}, \mathbf{w}) = \{\mathbf{W}\}^T[\mathbf{B}]^T[\bar{\mathbf{D}}][\mathbf{B}]\{\mathbf{U}\} \tag{3.15}$$

The linear functional can be written as :

$$\begin{aligned} F(\mathbf{w}) &= \int_A \mathbf{f}\mathbf{w}dA + \int_{\Gamma^N} \mathbf{T}\mathbf{w}ds \\ F(\mathbf{w}) &= \int_A \{\mathbf{w}\}^T\{\mathbf{f}\}dA + \int_{\Gamma^N} \{\mathbf{w}\}^T\{\mathbf{T}\}ds \end{aligned}$$

$$F(\mathbf{w}) = \{\mathbf{W}\}^T\Big[\int_A [\mathbf{\Phi}]^T\{\mathbf{f}\}dA + \int_\Gamma [\mathbf{\Phi}]^T\{\mathbf{T}\}ds\Big] \tag{3.16}$$

Now, substituting the above expressions for bilinear and linear functional , we get

$$\begin{aligned} \beta(\mathbf{u}_{FEM}, \mathbf{w}) &= F(\mathbf{w}) \\ \{\mathbf{W}\}^T\Big[\int_A [\mathbf{B}]^T[\bar{\mathbf{D}}][\mathbf{B}]dA\Big]\{\mathbf{U}\} &= \{\mathbf{W}\}^T\Big[\int_A [\mathbf{\Phi}]^T\{\mathbf{f}\}dA + \int_\Gamma [\mathbf{\Phi}]^T\{\mathbf{T}\}ds\Big] \end{aligned}$$

Since, $\{\mathbf{W}\}$ is arbitrary, we have

$$[\mathbf{K}]\{\mathbf{U}\} = \{\mathbf{F}\} \tag{3.17}$$

where $[\mathbf{K}]$ is the element stiffness matrix given by :

$$[\mathbf{K}] = \int_A [\mathbf{B}]^T[\bar{\mathbf{D}}][\mathbf{B}]dA \tag{3.18}$$

and $\{\mathbf{F}\}$ is the load vector given by :

$$\{\mathbf{F}\} = \int_A [\mathbf{\Phi}]^T\{\mathbf{f}\}dA + \int_\Gamma [\mathbf{\Phi}]^T\{\mathbf{T}\}ds \tag{3.19}$$

3.2.1 Computation of stiffness matrix and load vector

After expanding the terms of equation (3.18), the entries for element stiffness matrix can be written in the following form for a given i and j :

$$\begin{aligned} K_{(2i-1)(2j-1)} &= \int_A (\bar{Q}_{11}\Phi_{j,x}\Phi_{i,x} + \bar{Q}_{33}\Phi_{j,y}\Phi_{i,y})dA \\ K_{(2i-1)(2j)} &= \int_A (\bar{Q}_{12}\Phi_{j,y}\Phi_{i,x} + \bar{Q}_{33}\Phi_{j,x}\Phi_{i,y})dA \\ K_{(2i)(2j-1)} &= \int_A (\bar{Q}_{12}\Phi_{j,x}\Phi_{i,y} + \bar{Q}_{33}\Phi_{j,y}\Phi_{i,x})dA \\ K_{(2i)(2j)} &= \int_A (\bar{Q}_{22}\Phi_{j,y}\Phi_{i,y} + \bar{Q}_{33}\Phi_{j,x}\Phi_{i,x})dA \end{aligned}$$

Here i and j varies from 1 to $NDOF$ (where NDOF is the number of degrees of freedom). Similarly, from equation (3.19) we get

$$\begin{aligned} F_{(2i-1)} &= \int_A f_x\Phi_i dA + \int_\Gamma T_x\Phi_i ds \\ F_{(2i)} &= \int_A f_y\Phi_i dA + \int_\Gamma T_y\Phi_i ds \end{aligned}$$

3.3 Geometry mapping

Numerical integration of the stiffness matrix entries and the load vector entries necessitates the transformation of the physical coordinates (x, y) to the master element coordinates (ξ, η). Hence instead of defining the shape functions Φ_i in the physical coordinate system, it is defined in master element coordinates denoted by N_i. The geometry is expressed in terms of shape functions :

$$x = \sum_{i=1}^{3} x_i^e N_i \tag{3.20}$$

$$y = \sum_{i=1}^{3} y_i^e N_i \tag{3.21}$$

where x_i^e and y_i^e are the physical coordinates of the i-th node of the element e and N_i is the shape functions defined in master element coordinates (ξ, η).

Linear mapping

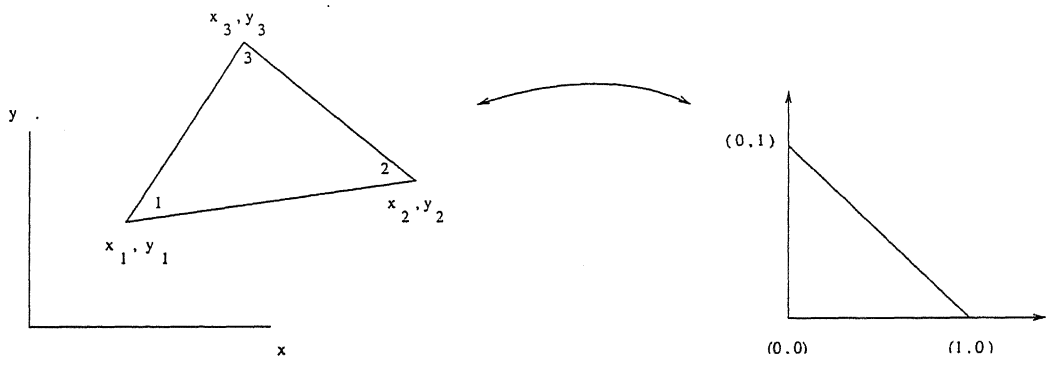

Figure 3.1: Linear mapping

Linear mapping is generally used when the sides of the physical elements are straight edges. Then the shape functions are given as :

$$\begin{aligned} N_1 &= 1 - \xi - \eta \\ N_2 &= \xi \\ N_3 &= \eta \end{aligned}$$

Substituting the above relations, we get

$$\begin{aligned} x &= x_1^e(1 - \xi - \eta) + x_2^e\xi + x_3^e\eta \\ y &= y_1^e(1 - \xi - \eta) + y_2^e\xi + y_3^e\eta \end{aligned}$$

or

$$\begin{Bmatrix} x - x_1^e \\ y - y_1^e \end{Bmatrix} = \begin{bmatrix} (x_2^e - x_1^e) & (x_3^e - x_1^e) \\ (y_2^e - y_1^e) & (y_3^e - y_1^e) \end{bmatrix} \begin{Bmatrix} \xi \\ \eta \end{Bmatrix} \tag{3.22}$$

$$\begin{Bmatrix} \xi \\ \eta \end{Bmatrix} = \frac{1}{|\mathbf{J}|} \begin{bmatrix} (y_3^e - y_1^e) & -(x_3^e - x_1^e) \\ -(y_2^e - y_1^e) & (x_2^e - x_1^e) \end{bmatrix} \begin{Bmatrix} (x - x_1^e) \\ (y - y_1^e) \end{Bmatrix}$$

where [J] is the jacobian matrix given by :

$$[\mathbf{J}] = \begin{bmatrix} (x_2^e - x_1^e) & (x_3^e - x_1^e) \\ (y_2^e - y_1^e) & (y_3^e - y_1^e) \end{bmatrix} \tag{3.23}$$

The derivatives of the shape functions are calculated using chain rule :

$$\begin{aligned} \frac{\partial \Phi_i}{\partial x} &= \frac{\partial N_i}{\partial \xi}\frac{\partial \xi}{\partial x} + \frac{\partial N_i}{\partial \eta}\frac{\partial \eta}{\partial x} \\ \frac{\partial \Phi_i}{\partial y} &= \frac{\partial N_i}{\partial \xi}\frac{\partial \xi}{\partial y} + \frac{\partial N_i}{\partial \eta}\frac{\partial \eta}{\partial y} \end{aligned}$$

The derivatives for linear transformation are given by :

$$\frac{\partial \xi}{\partial x} = \frac{1}{|\mathbf{J}|}(y_3^e - y_1^e) \tag{3.24}$$

$$\frac{\partial \xi}{\partial y} = -\frac{1}{|\mathbf{J}|}(x_3^e - x_1^e) \tag{3.25}$$

$$\frac{\partial \eta}{\partial x} = -\frac{1}{|\mathbf{J}|}(y_2^e - y_1^e) \tag{3.26}$$

$$\frac{\partial \eta}{\partial y} = \frac{1}{|\mathbf{J}|}(x_2^e - x_1^e) \tag{3.27}$$

Numerical integration

The numerical integration over a general triangle is achieved by mapping the triangle to a defined master element and then performing the area integral. The mapping can be either linear or quadratic or any order which depends on the geometry of the general element is described in the above paragraph.After transformation, the integral value is given by :

$$\begin{aligned} \int_{A^e} F(x,y)dxdy &= \int_A F(\xi,\eta)|\mathbf{J}|d\xi d\eta \\ &\simeq \frac{1}{2}\sum_{i=1}^{NINT} w(i)F(\xi_i,\eta_i)|\mathbf{J}| \end{aligned}$$

where A^e is the area of the physical element, A is the area of the master element and NINT is the number of integration points.

Chapter 4

Generalized finite element formulation

4.1 Introduction

In the standard finite element method, the approximate solution is constructed by employing piecewise polynomial function of degree p. A major drawback of this method is that for the domain with re-entrant corner (or crack), severe mesh refinement, near the vertex of the corner is required. Thus the size of computational problem increases. This is because the solution is very unsmooth in the vicinity of the crack tip. However in case of linearised elasticity based fracture mechanics, the representation of the unsmooth part of the solution is known in the vicinity of the crack tip, as a series. Hence, incorporating this special function in the finite element representation will significantly improve the quality of the finite element solution in the vicinity of the crack tip. Thus the necessity of the mesh refinement would be drastically reduced for this type of finite element analysis. Further, the critical parameter (for example the J integral) can be obtained more accuartely as compared to conventional finite element analysis. Below, a detailed outline of the generalized finite element method (GFEM) is given.

4.2 Construction of the conforming generalized finite element approximation

In this section, we describe how the finite element approximation can be generalized to include special functions. The standard shape functions used in finite elements result in mapped polynomials and are known to approximate smooth functions well. However, if the solution is known to be harmonic, it would be advantageous to use harmonic polynomials to form the basis. But the problem of continuity of approximation or conformity should be addressed properly to make sure that the approximation has finite energy. Conformity has been addressed in the standard finite element method (FEM) by constructing element shape functions in such a way that the proper number of degrees of freedom match at the boundaries of neighbouring elements and thus create a continuous approximation. Using any of the standard FEM elements and an associated family of shape functions of degree p, we can exactly represent all polynomials of degree p. These

shape functions are pasted together from neighbouring elements and form a basis by suppressing any linear dependencies, e.g., rigid body modes in elasticity. The resulting system of equations are solvable. The partition of unity method allows creation of conforming approximation using

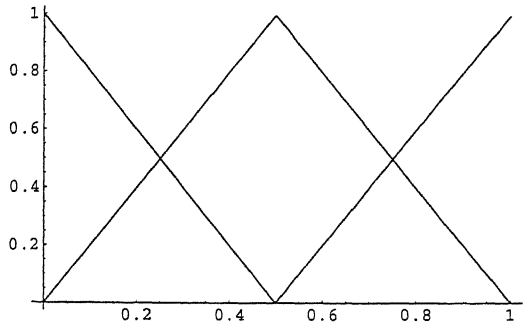

Figure 4.1: Linear support hat function

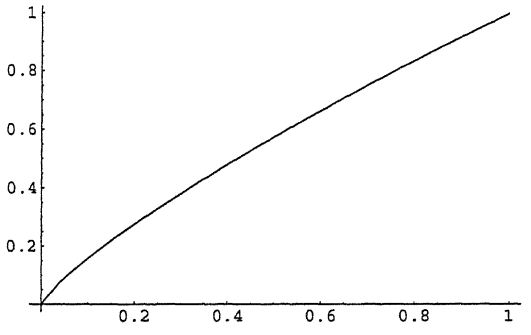

Figure 4.2: Special function to be used for enrichment for e.g., $x^{0.8}$

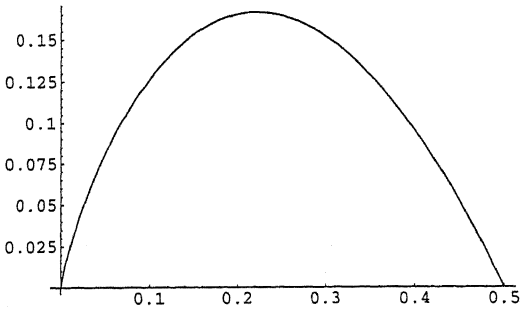

Figure 4.3: Generalized basis function given by $x^{0.8}(1-2x)$ over the domain $(0, 0.5)$

special functions. Given a set of overlapping subdomains or patches $\{\Omega_i\}$ (see figure 4.1) and a set of functions with desirable approximation properties associated with each patch $\Psi = \{\psi_j^i\}$, (see figure 4.2) we define the PUM approximate solution over the domain Ω (see figure 4.3) as

$$\mathbf{u}_{PUM} = \sum_i \Phi_i \Big(\sum_j a_j^i \psi_j^i \Big) \tag{4.1}$$

where $\psi_j^i(x,y)$ is a special function from the set $\{\psi^i\}$. The space Ψ_i is called the patch space. The a_j^i are the constant coefficients. The sequence of functions $\{\Phi_i\}$ (one for each patch of the set $\{\Omega_i\}$) is a partition of unity on Ω and serves to enforce continuity.
Although the partition can be constructed in any manner as long as it satisfies the definition, in the present work we construct it using linear hat functions over coarse patches of triangular elements (see for one dimension example figure 4.1 - 4.3). The patches $\{\Omega_i\}$ and each associated member of the sequence $\{\Phi_i\}$must satisfy the conditions stated below :

$$\{\Omega_i \text{ is an open cover of } \Omega,\}$$

$$\begin{aligned} \Phi_i &\in C^0 \ \forall \ i, && (4.2)\\ \sup\Phi_i &\in closure(\Omega_i) \ \forall \ i, && (4.3)\\ \sum_i \Phi_i &\equiv 1 \text{ on } \Omega, && (4.4)\\ \|\Phi_i\|_L^\infty &\leqq C_\infty, && (4.5) \end{aligned}$$

The displacement field, at a crack tip, is contained in the span of the following four functions :

$$\{\gamma(r,\theta)\} = \left\{\sqrt{r}\cos\frac{\theta}{2}, \sqrt{r}\sin\frac{\theta}{2}, \sqrt{r}\sin\frac{\theta}{2}\sin\theta, \sqrt{r}\cos\frac{\theta}{2}\sin\theta\right\} \tag{4.6}$$

These functions will be used to enrich the standard finite element shape functions to give better approximation. Although more general form of enrichment function can be used, we used the above span to enrich the shape function used by Belytschko et al. [4]. Thus we can completely generalize the finite element approximation, allowing any family of special functions to be mixed with the mapped polynomial shape functions. The generalized finite element approximation is given by

$$\mathbf{u}_{GFEM} = \sum_{i=1}^{n_{vert}} \Phi_i \Big(\sum_j^{n_E^i} a_j^i \psi_j^i \Big) + \sum_k^{n_{FEM}} u_k N_k \tag{4.7}$$

where n_{vert} is the number of hat functions at element vertices, n_i is the number of special functions in the patch space Ψ_i associated with the vertex and n_{FEM} is the number of finite element side modes and interior modes.
Note that the traditional FEM basis functions are evaluated on the master element (ξ,η) but the higher order special functions are expressed in terms of unmapped physical coordinate system of the problem (x,y).

4.3 Linear dependency

As mentioned earlier, the GFEM may lead to a singular stiffness matrix because of linear dependence of the local approximation functions. On the contrary, in traditional FEM the solution

corresponding to zero eigen value is removed by imposing essential boundary conditions. However this is not possible in GFEM because the eigen functions associated with the zero eigen value are not known generally. To solve such a linear system of equations one can use several methods like the perturbation approach [6]. In the present study, perturbation technique is incorporated in the solver code to solve such system of equations, though singularity does not arise in our case. When [A] is a singular matrix, then a particular solution can be obtained by :

$$[\mathbf{A}]_\varepsilon = [\mathbf{A}] + \varepsilon[\mathbf{I}]$$

where ε is the perturbation, usually taken very small and [I] is the identity matrix. Thus $[\mathbf{A}]_\varepsilon$ is positive definite matrix and can be inverted by any standard method.

4.4 Adaptive integration

Since in the present work we are enriching the usual finite element space with local asymptotic solution in the vicinity of crack tip which have singular derivatives at $r = 0$, we must take care of numerically integrating their entries in element stiffness matrix or load vector. This is done using adaptive gauss quadrature integration, in the elements where the special functions are employed. For all other elements the standard gauss quadrature rule is applied. In the following paragraph, adaptive integration scheme will be discussed elaborately.
The GFEM approximation will be defined as

$$\hat{N}_i(\xi,\eta) = r^{\frac{1}{2}} \cos\frac{\theta}{2} N_m(\xi,\eta)$$

where $N_m(\xi,\eta)$ is the traditional finite element shape function defined in the master element and $\hat{N}_i(\xi,\eta)$ is the new auxiliary shape function. Now to compute the stiffness entries, we need to find the derivatives of the auxiliary shape functions which we can find by applying chain rule.

$$\frac{\partial \hat{N}_i(\xi,\eta)}{\partial x} = \left[\frac{\partial N_m(\xi,\eta)}{\partial \xi}\frac{\partial \xi}{\partial x} + \frac{\partial N_m(\xi,\eta)}{\partial \eta}\frac{\partial \eta}{\partial x}\right] r^{\frac{1}{2}} \cos\frac{\theta}{2} + N_m(\xi,\eta)\frac{\partial}{\partial x}(r^{\frac{1}{2}} \cos\frac{\theta}{2})$$

So, the stiffness entries corresponding to the auxiliary degree of freedom involves singular derivatives. To compute the stiffness entries for such row and column which involves the auxiliary degree of freedom, we divide the master element into four equal parts and compute the area integral on each of the sub master element and added to give the total value for that element (see figure 4.4). This value is then checked with the value calculated in the previous iteration, if the error is within the range of the tolerance specified in the code then no further subdivisions are carried out and calculation of next stiffness entry is carried out. However, if the error is more than the tolerance specified then out of the four sub master element, the sub master element asociated with the crack tip is redivided into four equal triangles and the integrand is evaluated on each of the element parts and summed to give the total value (see figure 4.4). Special care

should be taken to ensure that the weighting factor of the standard gauss quadrature rule gets modified after a triangle is divided. For example, in the first iteration after division of the master element into four equal triangles the weighting function for all the sub master elements should be divided by four. While the situation in any other iteration greater than one is more complex, since it involves both the sub master elements obtained in the previous iteration and the integral domain obtained after the division of the triangle associated with the crack tip into four more parts. Hence special care should be taken so that all the previously divided elements which have not been subdivided should retain their weighting function pertaining to the previous iteration and for the triangle which has been sub divided, its weighting function should be divided by four again to get the weighting function for each of the sub divided triangles. In the present work a

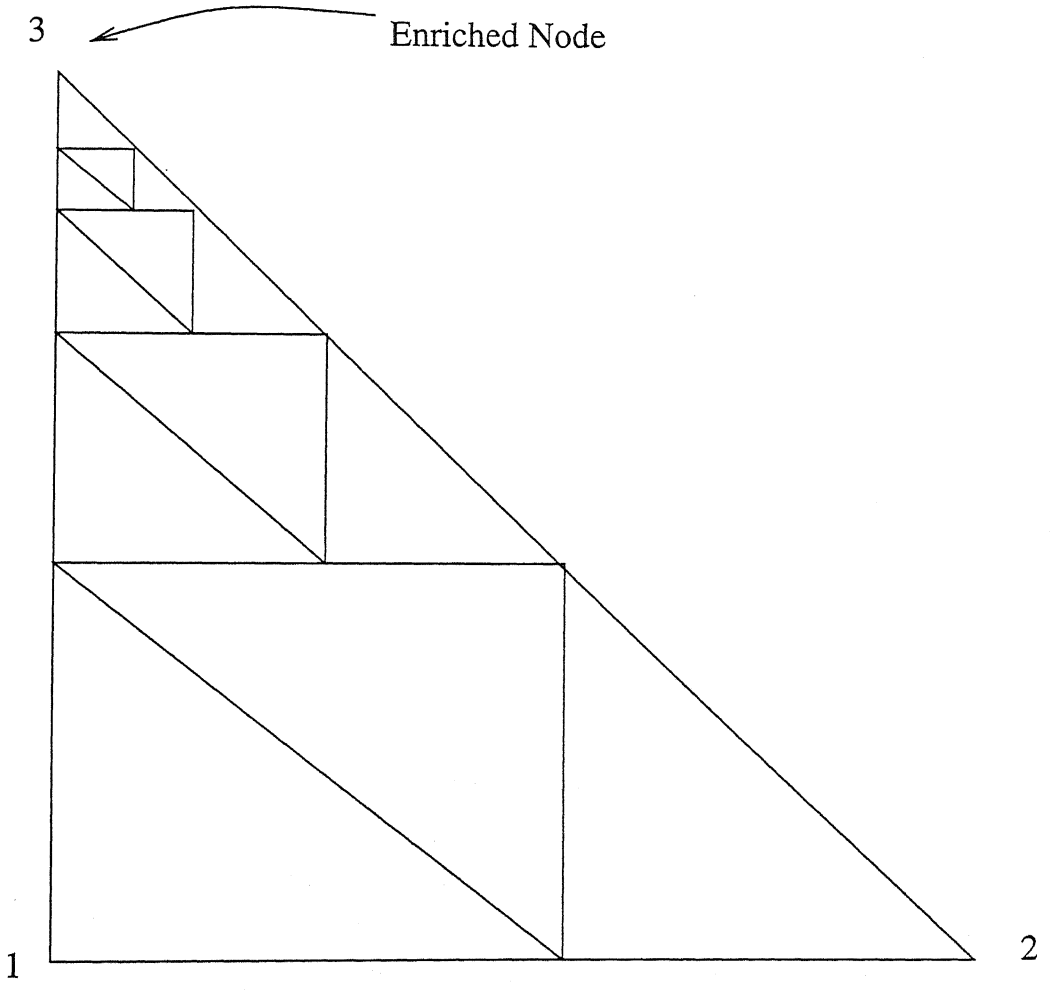

Figure 4.4: Scheme for Adaptive Integration

ninth order integration rule is applied which results in nineteen integration points. In each of the sub divided triangles, the same order integration rule is applied to maintain the simplicity of the code. An important aspect of the present adaptive integration procedure is that we apply the prior knowledge of the node corresponding to crack tip which has been enriched and subsequently

attack the node to achieve desired accuracy. This approach ensures that the stiffness entries are accurate. However one has to be cautious since the same integration rule is applied to each of the sub divided domain, proper care should be taken to transform the sub master element coordinate to the actual master element. This is due to the fact that the shape functions are defined in actual master element and not in the sub master element. This is taken care of by a linear map of the sub master element coordinates to the actual master element coordinates since the master element is an isoceles right angled traiangle having straight edges.
An important observation is that the present approach takes longer time for diagonal elements. This is due to the fact that the off-diagonal elements exhibit weaker singularity than the diagonal elements. In this work, we imposed a tolerance of 10^{-08}. Note that, we could have carried out a single computation of unsmooth integrand, and obtain the desired level of subdivision required in the master element, for elements at the crack tip. This can then be used to do the integration in one shot, for all the elements at the crack tip.

4.5 Solution technique

The solution phase of the finite element computer programs consists of three parts:

1. Assembly of the stiffness matrix and load vector from the element level stiffness matrices and load vectors;

2. Enforcement of the principal boundary conditions, and

3. Solution of the system of simultaneous equation.

In engineering problems the size of the system of equations is generally quite large, and the entire global stiffness matrix cannot be stored in runtime memory, even if only the non-zero entries are stored. It is important to design the solution algorithm so that the arithmetic operations in the solution phase can be performed as efficiently as possible.
In the present work, we have used the *frontal solution method.* The frontal solution method was proposed by *Irons* [12]. Its main feature is that the order in which the gaussian elemination is performed is element oriented rather than node oriented. It is not necessary to number nodes for minimum bandwidth. Another important feature of this method is that assembly of the stiffness matrix and the gaussian elimination is carried out concurrently.

Chapter 5

Numerical results for stationary crack

In the present chapter we will discuss the results obtained. Both straight and arbitrary shaped crack segments were considered. Initially a comparison is drawn between FEM solution and GFEM solution to prove the efficiency of the proposed methodology. The cases were solved using hierarchic shape functions of order p ($p \leq 3$). This could be very easily extended to even higher order approximating polynomial. In all the cases, the enrichment functions used were conforming to the one proposed by Fleming et al [4]. However more general enrichment functions could be employed.

Crack modelling

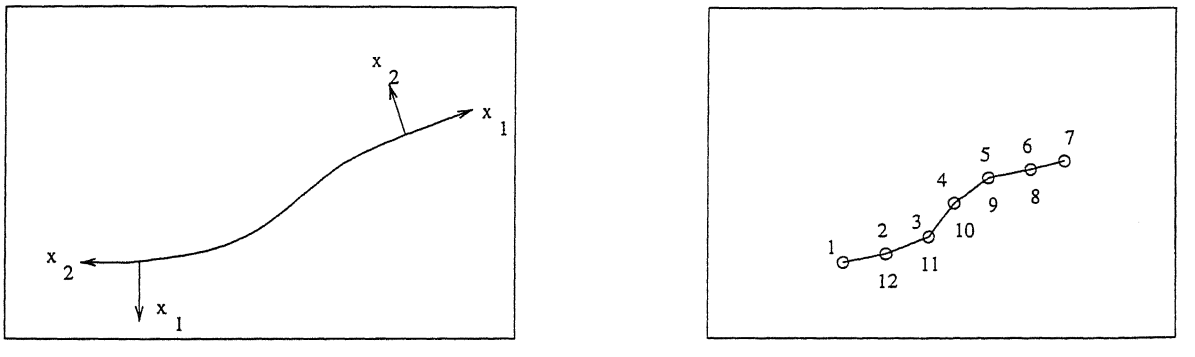

Actual Crack

Modelled Crack

Figure 5.1: Crack modelling

In the present work, any arbitrary shaped crack is modelled as a series of straight line segment connected at nodes as shown in figure 5.1. To ensure the discontinuity along the crack faces, two nodes were created at the same position one on the upper surface of the crack and the another one on the lower surface. This ensures that the element discretization above and below the crack faces are independent of each other. The local coordinates at the crack tip are taken parallel to

the end line segment(see figure 5.1).

In all the cases the full plate analysis is done to elaborate the computational strategy in case of multiple singularities in the domain. For all the problems, plane strain condition is chosen and the following material properties, boundary conditions and loads are taken :

Material properties : $E = 100\ kpsi$ and $\nu = 0.3$

Boundary conditions : Four corner nodes fixed

Traction : $T_y = 1.0\ psi$ on the opposite edges

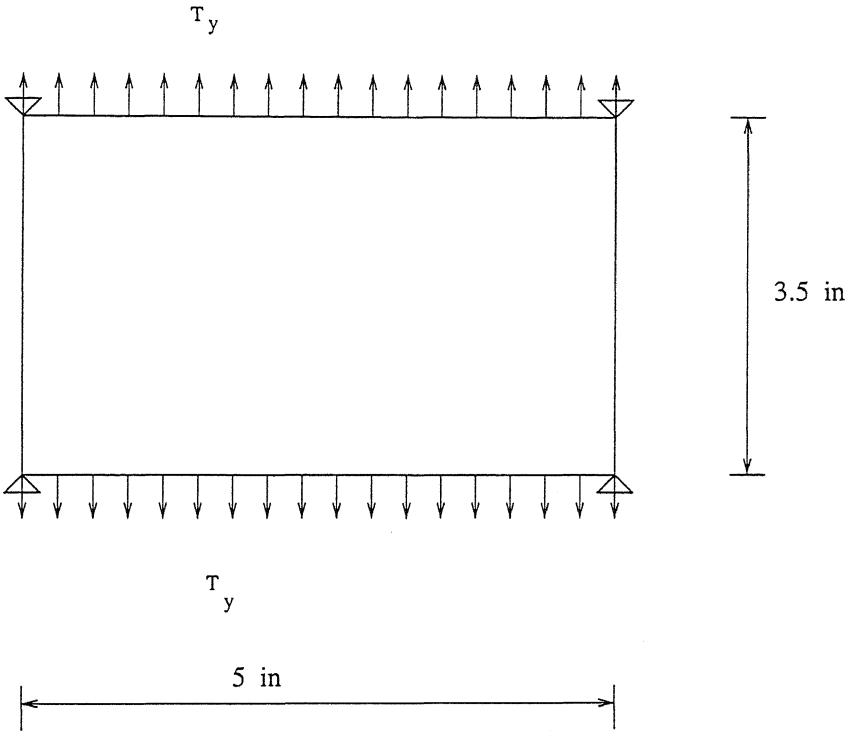

Figure 5.2: Boundary conditions and loading conditions

The plate is taken to be of dimensions 5in $\times$ 3.5in (as shown in figure 5.2).

Problem 1 : Centrally located straight edge small crack

A center cracked plate with the following parameters is analysed :

$$\text{Domain} = 5 \times 3.5\ in^2$$
$$\text{Crack Length} = 0.5\ in$$

Two different mesh is employed, one is coarser(see figure 5.3) and the other one is finer(see figure 5.4). The computed values of the various crack parameters using either the conventional FEM or GFEM are reported in table 5.1 and 5.2. Note that in the computation of stress intensity factors, the contour is taken to correspond to the outer boundaries of either one layer of elements adjacent to the crack tip or two layer of elements.

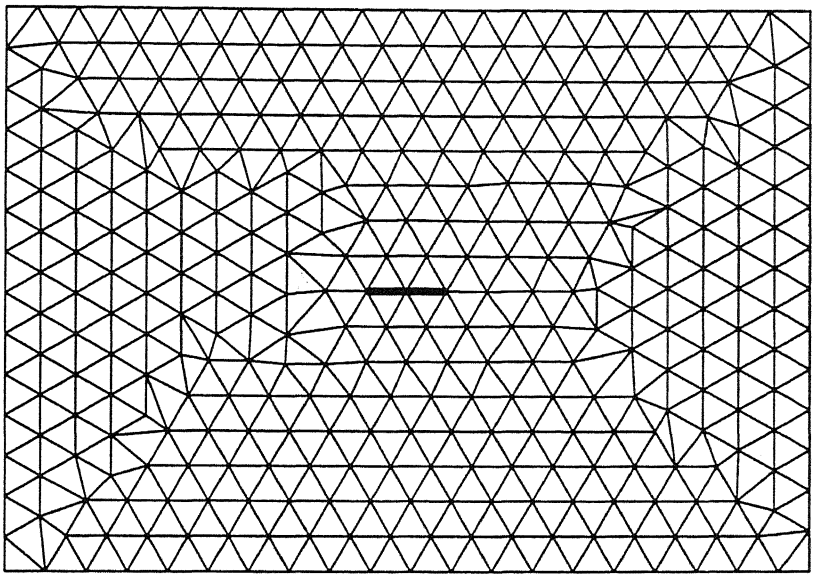

Figure 5.3: Straight edge crack of length 0.5in with coarse mesh

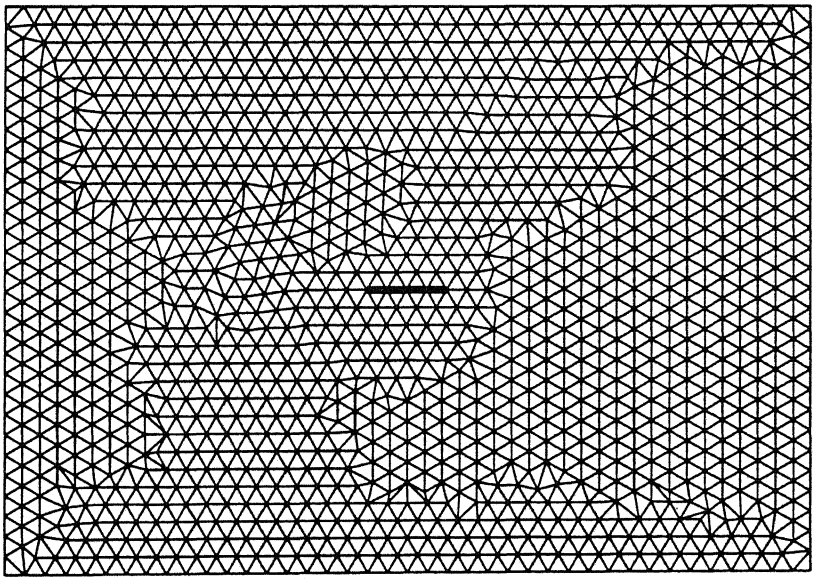

Figure 5.4: Straight edge crack of length 0.5in with fine mesh

Table 5.1: Stress intensity factors computed for coarse mesh

Scheme	No. of Elements	Order of Shape Functions , p	Layer of Element to compute Interaction Integral	K_I in $psi\sqrt{in}$	K_{II} in $psi\sqrt{in}$
FEM	634	1	1	0.871998271	-0.00186705222
				0.871918492	-0.00213316604
GFEM	634	1	1	0.764668694	-0.0017483637
				0.766995734	-0.00157027579
FEM	634	2	1	0.82840364	-0.000819087014
				0.828413002	-0.000812332551
GFEM	634	2	1	0.978282491	-0.00123810708
				0.978622215	-0.00106178627

Table 5.2: Stress intensity factors computed for refined mesh

Scheme	No. of Elements	Order of Shape Functions , p	Layer of Element to compute Interaction Integral	K_I in $psi\sqrt{in}$	K_{II} $psi\sqrt{in}$
FEM	2564	1	1	0.626637336	-0.000337844132
				0.626767391	-0.000283837087
GFEM	2564	1	1	0.500493715	-0.000460228968
				0.50052228	-0.000217512687
FEM	2564	1	2	0.849307746	-0.000258345046
				0.849500731	-0.000256760112
GFEM	2564	1	2	0.855961206	-0.00104771529
				0.855961206	-0.000787968813

Infinite Plate in Mode I Loading	$K_I = 0.895\ psi\sqrt{in}$	$K_{II} = 0\ psi\sqrt{in}$

Discussion

1. The theoretical value of K_I and K_{II} for finite plate, after applying finite plate corrections, are $K_I = 0.895$ and $K_{II} = 0$. The value obtained by GFEM and FEM with either $p = 2$ and one layer or $p = 1$ and two layer are sufficiently close to the theoretical values.

2. The contour integral method applied in the study is highly sensitive to the distance of the contour from the crack tip. As the contour is brought closer to the crack tip, the quality of the extracted stress intensity factor deteriorates.

3. The stiffness intensity factors obtained at the left crack tip and right crack tip do not match exactly because of the lack of symmetry in the mesh used. Though, it should be noted that the discrepancy is insignificant.

4. For coarse mesh, the results are not good beacause the crack length is too small. The contour integral employed in the extraction of the stress intensity factors will be severely affected by the neighbouring crack tip. This is the reason that Fleming et al [4] suggested mesh refinement at the crack root for getting better results.

Problem 2 : Centrally located straight edge long crack

In this problem a centre cracked plate with the following parameters is analysed :

$$\text{Domain} = 5 \times 3.5 \ in^2$$
$$\text{Crack Length} = 1.0 \ in$$

A different crack length is chosen to demonstrate the effect of increasing crack length on the solution and how the higher order shape function affects the solution.In this problem the mesh employed is coarsh(see figure 5.5) The computed values of the stress intensity factors are reported in table 5.3 and 5.4

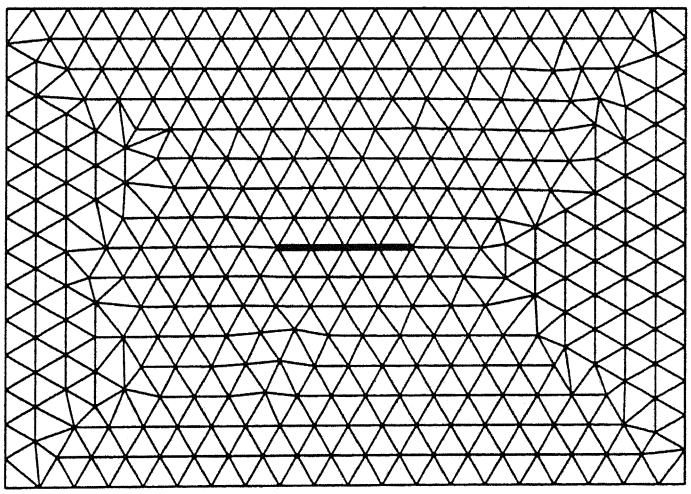

Figure 5.5: Straight edge crack of length of 1in

Table 5.3: Stress intensity factors computed for p = 1

Scheme	No. of Elements	Order of Shape Functions , p	Layer of Element to compute Interaction Integral	K_I in $psi\sqrt{in}$	K_{II} $psi\sqrt{in}$
FEM	628	1	1	0.90438288	-0.00278504271
				0.904393975	-0.0028196911
GFEM	628	1	1	0.744402238	-0.00184098385
				0.74466355	-0.00191254745
FEM	628	1	2	0.764668694	-0.00236289666
				0.766995734	-0.0023754772
GFEM	628	1	2	1.25931867	-0.00262408054
				1.26092989	-0.00329535918

Table 5.4: Stress intensity factors computed for p = 2

Scheme	No. of Elements	Order of Shape Functions , p	Layer of Element to compute Interaction Integral	K_I in $psi\sqrt{in}$	K_{II} $psi\sqrt{in}$
FEM	628	2	1	0.841305802	-0.0017483637
				0.841326947	-0.00157027579
GFEM	628	2	1	0.969028848	-0.001050745056
				0.968735869	-0.00149841222
FEM	628	2	2	1.21598151	-0.0017483637
				1.21636486	-0.00157027579
GFEM	628	2	2	1.27639092	-0.00104771529
				1.27570483	-0.000787968813

Infinite plate in Mode I loading	$K_I = 1.28$ $psi\sqrt{in}$	$K_{II} = 0$ $psi\sqrt{in}$

Discussion

1. For $p = 1$, when the contour corresponds to two layer of elements, GFEM is very accurate while the standard FEM is not. Further using one layer of elements around the crack tip seems to be inefficient for the extraction of stress intensity factors.

2. For $p = 2$, GFEM is clearly far superior to standard FEM.

3. Note that in this problem, the interference from the neighbouring crack tip is very small leading to more accurate extracted quantities.

4. Inspite of a coarse unsymmetric mesh, the left and right stress intensity factor have insignificant mismatch.

Problem 3 : Arbitrary shaped crack

An arbitrary shaped crack with the following parameters is analysed :

$$\begin{aligned} \text{Domain} &= 5 \times 3.5 \ in^2 \\ \text{Crack Segment :} & \\ \text{node1} &= (2.00, 1.70) \\ \text{node2} &= (2.25, 1.70) \\ \text{node3} &= (2.50, 1.80) \\ \text{node4} &= (2.75, 1.80) \end{aligned}$$

The plate with the crack is shown in figure 5.6. The computed stress intensity factors are reported in table 5.5.

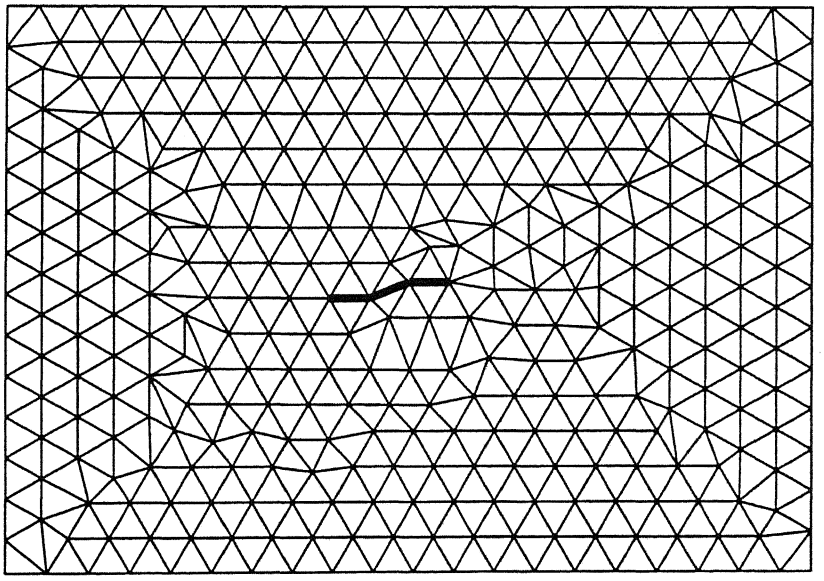

Figure 5.6: Problem 3

Table 5.5: Stress intensity factors computed for different p

Scheme	No. of Elements	Order of Shape Functions , p	Layer of Element to compute Interaction Integral	K_I in $psi\sqrt{in}$	K_{II} $psi\sqrt{in}$
GFEM	636	1	1	0.990401579	0.0154856607
				0.982036791	0.010429162
GFEM	636	2	1	1.2372214	0.0320909648
				1.24435412	0.0309407329
GFEM	636	3	1	1.20827447	0.0536397577
				1.19315666	0.022451595

Discussion

1. The stress intensity factors calculated for $p = 2$ and $p = 3$ are quite close and seems to converge (i.e. discrepancy is less than 5 pc).

2. Note that the K_{II} is essentially zero as compared to K_I and the crack will tend to grow straight. The left and the right stress intensity factor do not match because mesh is crude and unsymmetric, however, the discrepancy is minimal.

3. To improve the result, one or two level of mesh refinemnet near the crack tip is desirable.

Problem 4 : Arbitrary shaped crack

An arbitrary shaped crack with the following parameters is analysed :

$$\text{Domain} = 5 \times 3.5\ in^2$$

Crack Segment :

$$\text{node1} = (2.00, 1.70)$$
$$\text{node2} = (2.25, 1.72)$$
$$\text{node3} = (2.50, 1.75)$$
$$\text{node4} = (2.75, 1.70)$$
$$\text{node5} = (3.00, 1.75)$$

The arbitrary shaped crack is modelled as shown in figure 5.7. The computed stress intensity factors are reported in table 5.6 and 5.7.

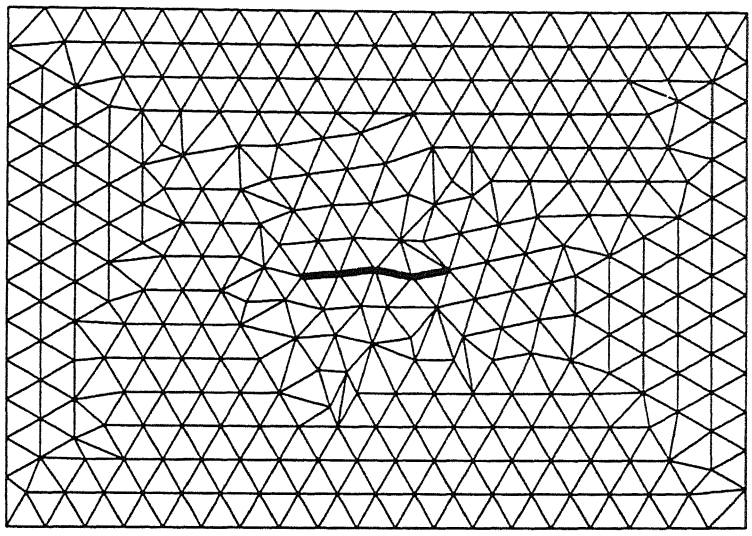

Figure 5.7: Problem 4

Table 5.6: Stress intensity factors computed for one layer

Scheme	No. of Elements	Order of Shape Functions , p	Layer of Elements to compute Interaction Integral	K_I in $psi\sqrt{in}$	K_{II} $psi\sqrt{in}$
GFEM	584	1	1	1.13418414	-0.00521811786
				1.08020361	-0.0412967273
GFEM	584	2	1	1.28536871	0.0419222697
				1.28719329	-0.063198877
GFEM	584	3	1	1.47696526	-0.0364505828
				1.41330589	0.027973453

Table 5.7: Stress intensity factors computed for two layer

Scheme	No. of Elements	Order of Shape Functions , p	Layer of Elements to compute Interaction Integral	K_I in $psi\sqrt{in}$	K_{II} $psi\sqrt{in}$
GFEM	584	1	2	1.5457882	-0.051235026
				1.56144341	0.0193207251
GFEM	584	2	2	1.4236723	-0.0542374126
				1.38937786	0.0665384271

Discussion

1. The results for 1 layer of elements is quite poor. However for $p = 3$ the results seem to be close to that obtained from extraction using two layer of elements around the crack tip.

2. Again in this case K_{II} is negligible because the crack behaves like a centrally placed crack.

Problem 5 : Crack growth for two symmetrically located crack

The growth of two symmetrically placed straight cracks with the following initial parameters is analysed here and the corresponding position of the cracks are shown in figure (5.8 - 5.11).

$$\begin{aligned}
\text{Domain} &= 5 \times 3.5\ in^2 \\
\text{Crack Profile 1 :} & \\
\text{node1} &= (1.500, 1.75) \\
\text{node2} &= (1.625, 1.75) \\
\text{node3} &= (1.750, 1.75) \\
\text{node4} &= (1.875, 1.75) \\
\text{node5} &= (2.000, 1.75) \\
\text{Crack Profile 2 :} & \\
\text{node1} &= (3.000, 1.75) \\
\text{node2} &= (3.125, 1.75) \\
\text{node3} &= (3.250, 1.75) \\
\text{node4} &= (3.375, 1.75) \\
\text{node5} &= (3.500, 1.75)
\end{aligned}$$

The purpose of the present problem is to estimate the robustness of the code for moving geometry. Here in each step, the crack length gets increased and the analysis is repeated. The crack extension direction is determined according to maximum tangential stress criterion detailed earlier in chapter 2. The extracted stress intensity factors for different p values are reported in table 5.8 - 5.13.

Step 1

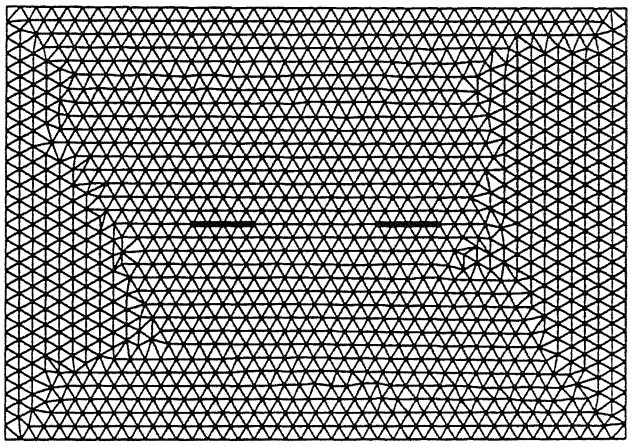

Figure 5.8: Problem 5 crack growth step 1

Table 5.8: Stress intensity factors computed at the end of step 1 with p = 1

Crack	No. of Elements	Order of Shape Functions , p	Layer of Elements to compute Interaction Integral	K_I in $psi\sqrt{in}$	K_{II} $psi\sqrt{in}$
1	2564	1	2	0.827900965	-0.000352688633
				0.85007153	-0.000317667391
2	2564	1	2	0.850005244	-0.000285569277
				0.827116411	-0.0000478630334

Table 5.9: Stress intensity factors computed at the end of step 1 with p = 2

Crack	No. of Elements	Order of Shape Functions , p	Layer of Elements to compute Interaction Integral	K_I in $psi\sqrt{in}$	K_{II} $psi\sqrt{in}$
1	2562	2	2	0.853412354	-0.000240084291
				0.869690615	-0.000255675898
2	2562	2	2	0.869697323	-0.000280393539
				0.853348802	-0.0000264159494

Step 2

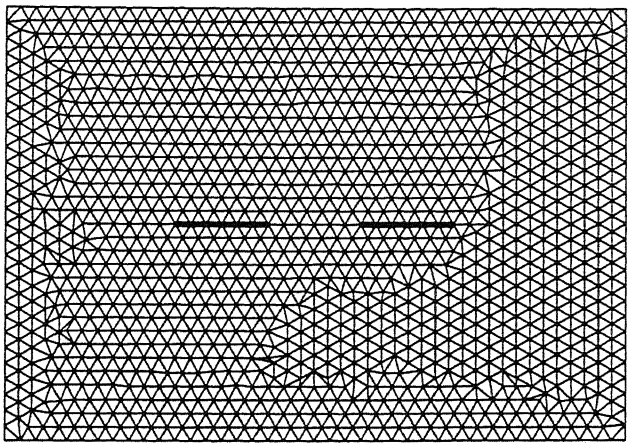

Figure 5.9: Problem 5 crack growth step 2

Table 5.10: Stress intensity factors computed at the end of step 2 with p = 1

Crack	No. of Elements	Order of Shape Functions , p	Layer of Element to compute Interaction Integral	K_I in $psi\sqrt{in}$	K_{II} $psi\sqrt{in}$
1	2564	1	2	0.820305226	-0.000301340611
				0.86535299	-0.000294438658
2	2564	1	2	0.865398794	-0.000570112828
				0.819049369	0.00263806512

Table 5.11: Stress intensity factors computed at the end of step 2 with p = 2

Crack	No. of Elements	Order of Shape Functions , p	Layer of Elements to compute Interaction Integral	K_I in $psi\sqrt{in}$	K_{II} $psi\sqrt{in}$
1	2560	2	2	0.848856914	-0.000126843033
				0.883541027	-0.000481974206
2	2560	2	2	0.881666649	-0.000156524428
				0.85113107	-0.000796571682

Step 3

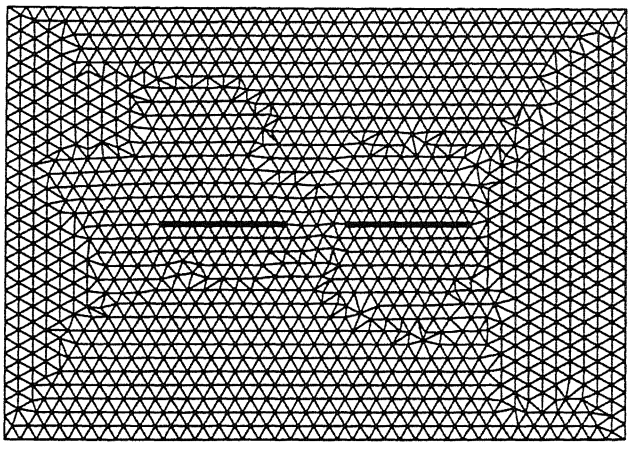

Figure 5.10: Problem 5 crack growth step 3

Table 5.12: Stress intensity factors computed at the end of step 3 with p = 1

Crack	No. of Elements	Order of Shape Functions , p	Layer of Element to compute Interaction Integral	K_I in $psi\sqrt{in}$	K_{II} $psi\sqrt{in}$
1	2510	1	2	0.912694996	-0.000292969031
				0.964575631	-0.00703674212
2	2510	1	2	0.918500545	-0.00261285263
				0.829219297	-0.00526810027

Table 5.13: Stress intensity factors computed at the end of step 3 with p = 2

Crack	No. of Elements	Order of Shape Functions , p	Layer of Elements to compute Interaction Integral	K_I in $psi\sqrt{in}$	K_{II} $psi\sqrt{in}$
1	2566	2	2	0.911692321	-0.000531385793
				1.00692173	-0.00147615579
2	2566	2	2	1.00926826	-0.000218973043
				0.921226773	0.00378581801

Final step

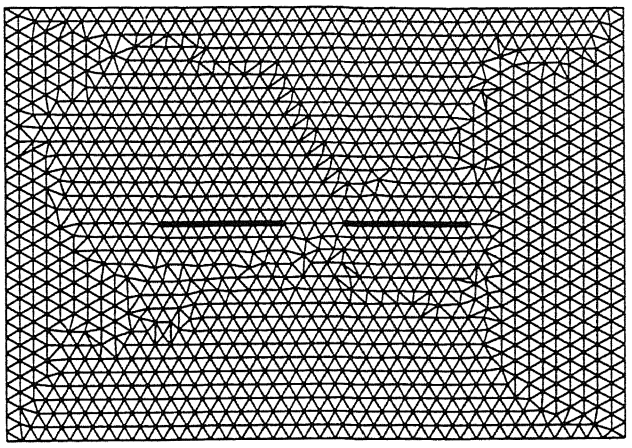

Figure 5.11: Problem 5 crack growth step 4

Discussion

1. Following the theoretical analysis, geometry and location of the crack, both the crack should propagate along a straight line. This is what we get out of our numerical analysis.
2. As the crack grows, the interaction between two cracks become more severe leading to an increase in stress intensity factor.
3. The crack propagation is stopped prior to merger because of the limitations of the current meshing process.

Problem 6 : crack growth for two arbitrarily located crack

In this problem two cracks are considered. However the cracks are located off center as shown in the figure(5.12). The details of the domain and the crack geometry are as follows :

$$\text{Domain} = 5 \times 3.5 \text{ in}^2$$

Crack Profile 1 :

$$\text{node1} = (1.500, 1.25)$$
$$\text{node2} = (1.625, 1.25)$$
$$\text{node3} = (1.750, 1.25)$$
$$\text{node4} = (1.875, 1.25)$$
$$\text{node5} = (2.000, 1.25)$$

Crack Profile 2 :

$$\text{node1} = (3.000, 2.25)$$
$$\text{node2} = (3.125, 2.25)$$
$$\text{node3} = (3.250, 2.25)$$
$$\text{node4} = (3.375, 2.25)$$
$$\text{node5} = (3.500, 2.25)$$

Each of the crack segment is taken as a series of line segments joining the above 5 nodes. After each step of iteration, the crack profiles are given proper crack extension in the right direction and the whole analysis is repeated. The computed stress intensity factors at the end of each step are reported in the table 5.14 - 5.23. The corresponding crack geometries at the beginning of each step are shown in figure (5.12 - 5.21).

Step 1

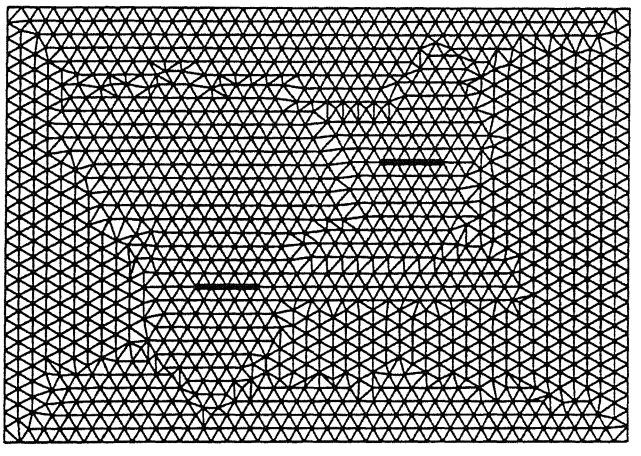

Figure 5.12: Problem 5 crack growth step 1

Table 5.14: Stress intensity factors computed at the end of step 1

Crack	No. of Elements	Order of Shape Functions , p	Layer of Element to compute Interaction Integral	K_I in $psi\sqrt{in}$	K_{II} $psi\sqrt{in}$
1	2584	1	2	0.835341791 0.850736133	0.0121879137 0.0113071723
2	2584	1	2	0.850696036 0.834182778	0.0113071723 0.0121700265

Step 2

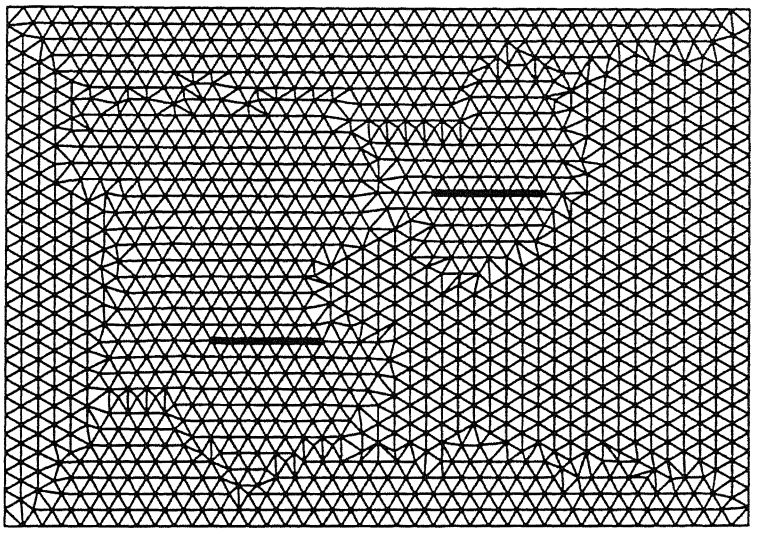

Figure 5.13: Problem 6 crack growth step 2

Table 5.15: Stress intensity factors computed at the end of step 2

Crack	No. of Elements	Order of Shape Functions , p	Layer of Element to compute Interaction Integral	K_I in $psi\sqrt{in}$	K_{II} $psi\sqrt{in}$
1	2596	1	2	0.830585879	0.00567496787
				0.851276091	-0.00508734123
2	2596	1	2	0.864274472	0.00791880615
				0.828841718	0.00307971677

Step 3

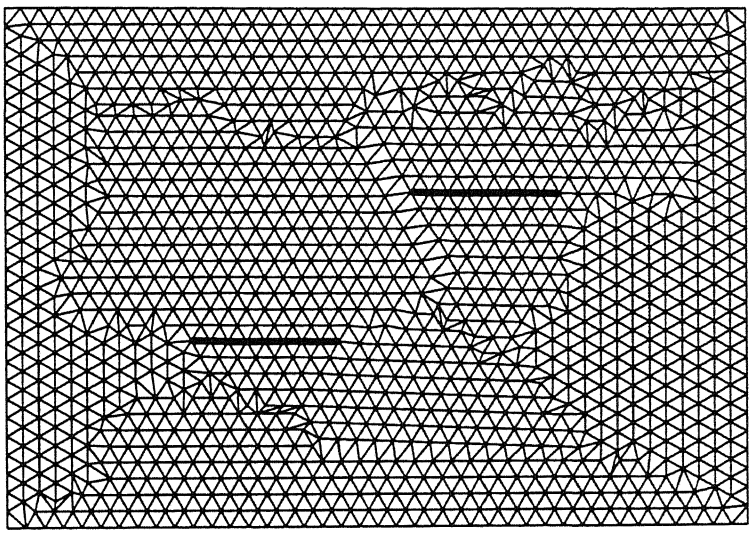

Figure 5.14: Problem 6 crack growth step 3

Table 5.16: Stress intensity factors computed at the end of step 3

Crack	No. of Elements	Order of Shape Functions , p	Layer of Element to compute Interaction Integral	K_I in $psi\sqrt{in}$	K_{II} $psi\sqrt{in}$
1	2578	1	2	1.00135083 1.09011459	-0.00158095561 -0.0132891375
2	2578	1	2	1.093026525 1.02283768	0.00643484579 0.00345989243

Step 4

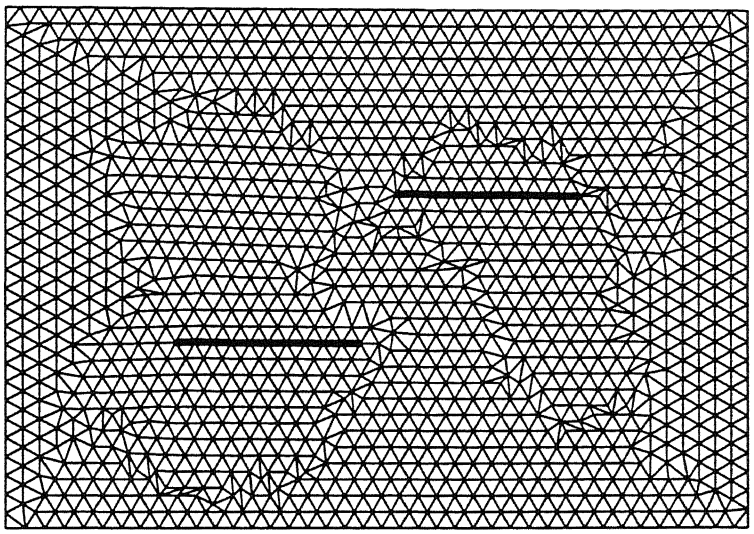

Figure 5.15: Problem 6 crack growth step 4

Table 5.17: Stress intensity factors computed at the end of step 4

Crack	No. of Elements	Order of Shape Functions , p	Layer of Element to compute Interaction Integral	K_I in $psi\sqrt{in}$	K_{II} $psi\sqrt{in}$
1	2570	1	2	1.36818268	-0.0211871321
				1.48479463	-0.0986211241
2	2570	1	2	1.4507246	-0.0194111176
				1.36069751	-0.000822044013

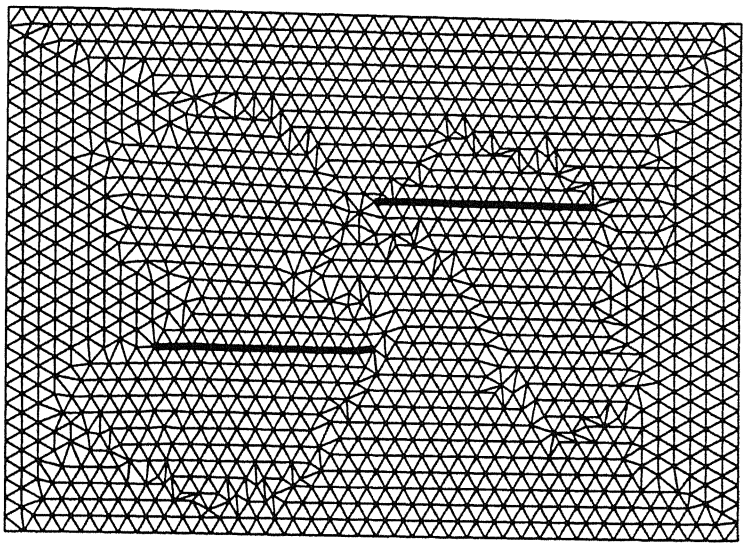

Figure 5.16: Problem 6 crack growth step 5

Table 5.18: Stress intensity factors computed at the end of step 5

Crack -	No. of Elements	Order of Shape Functions , p	Layer of Element to compute Interaction Integral	K_I in $psi\sqrt{in}$	K_{II} $psi\sqrt{in}$
1	2570	1	2	1.71884708	-0.0403886554
				1.86253646	-0.0604739141
2	2570	1	2	1.84575045	-0.200539113
				1.66395861	-0.117210394

Step 6

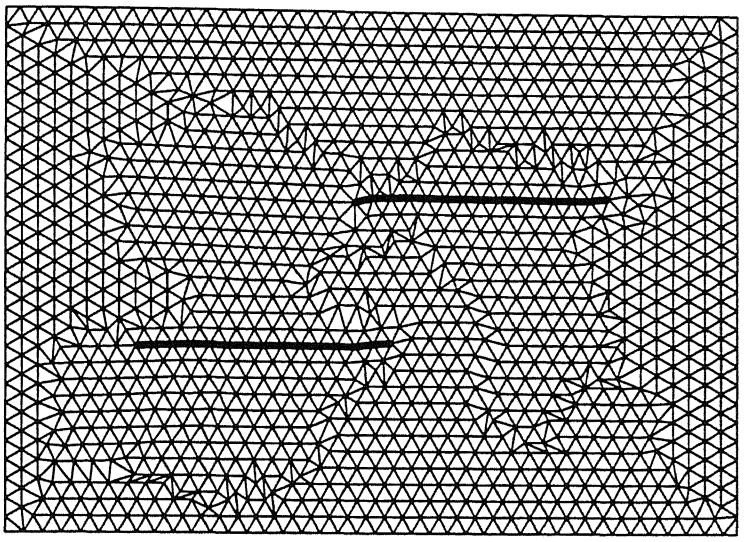

Figure 5.17: Problem 6 crack growth step 6

Table 5.19: Stress intensity factors computed at the end of step 6

Crack	No. of Elements	Order of Shape Functions , p	Layer of Element to compute Interaction Integral	K_I in $psi\sqrt{in}$	K_{II} $psi\sqrt{in}$
1	2582	1	2	2.02041082	-0.0529359263
				2.19797146	-0.313187923
2	2582	1	2	2.126893	-0.336561875
				2.09673951	-0.0556087537

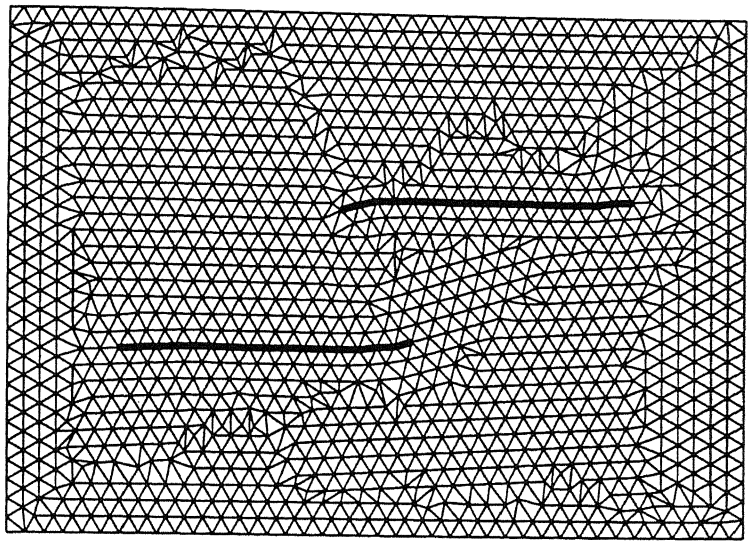

Figure 5.18: Problem 6 crack growth step 7

Table 5.20: Stress intensity factors computed at the end of step 7

Crack	No. of Elements	Order of Shape Functions , p	Layer of Element to compute Interaction Integral	K_I in $psi\sqrt{in}$	K_{II} $psi\sqrt{in}$
1	2580	1	2	2.48713937	-0.234273036
				2.56750505	-0.308852834
2	2580	1	2	2.43620877	-0.309309869
				2.44884128	-0.23661355

Step 8

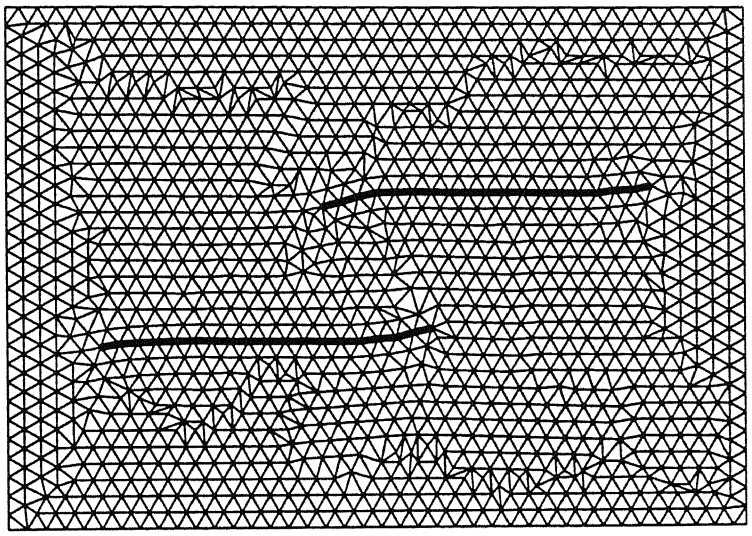

Figure 5.19: Problem 6 crack growth step 8

Table 5.21: Stress intensity factors computed at the end of step 8

Crack	No. of Elements	Order of Shape Functions , p	Layer of Element to compute Interaction Integral	K_I in $psi\sqrt{in}$	K_{II} $psi\sqrt{in}$
1	2592	1	2	2.94236899 2.6786357	-0.324194315 -0.315583614
2	2592	1	2	2.72784844 2.90369245	-0.491364253 -0.276572426

Step 9

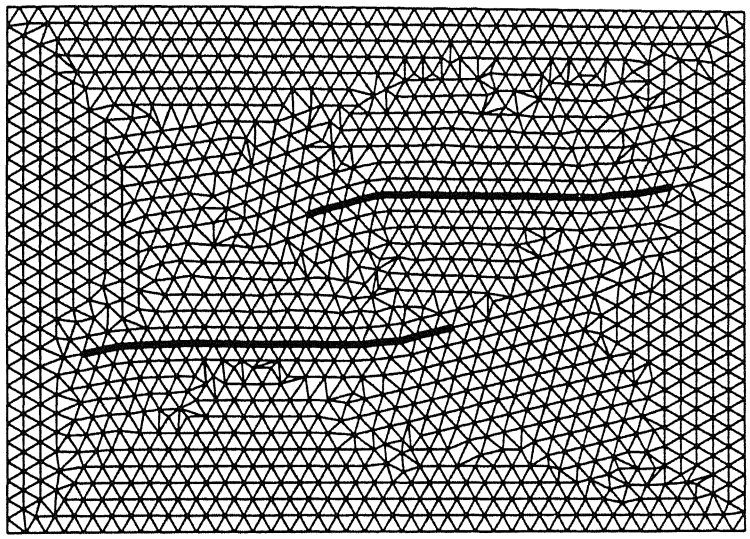

Figure 5.20: Problem 6 crack growth step 9

Table 5.22: Stress intensity factors computed at the end of step 9

Crack	No. of Elements	Order of Shape Functions , p	Layer of Element to compute Interaction Integral	K_I in $psi\sqrt{in}$	K_{II} $psi\sqrt{in}$
1	2572	1	2	3.30572489	-0.402490819
				2.97397514	-0.428100794
2	2572	1	2	2.98920629	-0.354454145
				3.22757431	-0.445701305

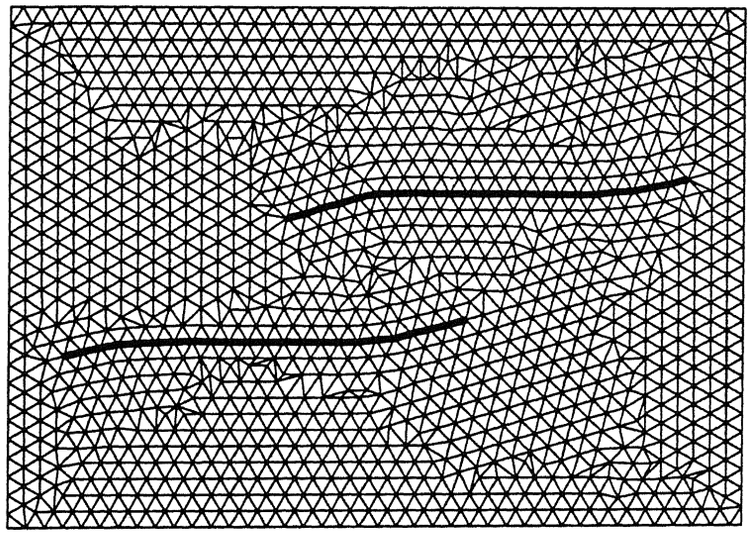

Figure 5.21: Problem 6 crack growth step 10

Table 5.23: Stress intensity factors computed at the end of step 10

Crack	No. of Elements	Order of Shape Functions , p	Layer of Element to compute Interaction Integral	K_I in $psi\sqrt{in}$	K_{II} $psi\sqrt{in}$
1	2560	1	2	3.65941563	-0.513562382
				3.21282555	-0.270626624
2	2560	1	2	3.17263255	-0.394161767
				3.71137782	-0.449254288

Discussion

1. A close look at the problem reveals that the crack positions are unaltered by a rotation of the domain by 180°. So one would expect the cracks to propagate in a self similar manner. The numerical results demonstrate that indeed it is true.

2. As the cracks grow, the interaction between the two cracks increases leading to an increase in the observed stress intensity factors.

3. The cracks tend to turn towards each other and towards the fixed boundary points at the two ends. This confirms with the observed photoelastic data for similar experiment as well as to the intuitive reasoning that near the boundary, the crack will tend to grow towards the region of high stress concentration.

4. The mixed mode stress intensity factor is mainly K_I dominated. $Mode\ II$ is important from the point of view of the orientation of the crack growth direction. The crack turns primarily due to K_{II}.

Chapter 6

Closure

6.1 Summary

In the present work, we developed a general computational code to model crack growth. The following conclusions can be drawn based on the present work :

1. The presence of multiple singularities in the domain has been successfully addressed. However more detailed analysis is to be done to improve the results further.

2. The generalized finite element is superior than the standard finite element solution.

3. The present approach has been extended to arbitrary shaped crack.

4. Mesh refinement is necessary in some cases, as in problem 1, where due to small crack length the local disturbance from the nearby cracktip is affecting the solution.

5. The stress intensity factors calculated from the interaction integral computed along the two layer of elements around the crack tip yield better results.

6. Higher order shape functions along with little mesh refinement could be very effective tool to characterise the crack parameters.

6.2 Suggestions for future work

1. The major difficulty in crack growth modelling in any of the finite element approach is to generate a mesh at each step conforming to the crack surface. The present study uses automatic mesh generator in crude form. The mesh generator should be improved by incorporating sub-domain wise meshing. The whole domain could be divided into a number of sub domains such that the crack surface falls on one of the boundary. This excludes the possiblity of any internal cut-outs.

2. In the present work, we have enriched only the node sitting at the crack tip. This could be extended to enrich the whole zone around the crack tip. This will improve the results immensely.

3. The enrichment functions used in the present method is as proposed by Fleming et al [4]. However, much better results could be obtained by using the exact functions as derived for re-entrant corner.

4. Mesh refinement might be necessary in some cases particularly when the cracks come closer to each other. This would improve the results immensely. Instead of mesh refinement throughout the whole domain, it is better to refine only those elements which are associated with the node sitting on the crack tip.

5. In the present study contour form of interaction integral is applied to extract stress intensity factor in mixed mode analysis. However, domain form of interaction integral based on cut-off function method (see [12]) or contour form of interaction integral around an annular ring surrounding the crack tip (see [12]) would yield better results.

Bibliography

[1] I. Babuska and J. M. Melenk, " The Partition of Unity Method ", *International Journal for Numerical Methods in Engineering*, Vol. 40, 727 -758, 1997

[2] C. Duarte and J. Oden, " hp clouds - a meshless method for boundary value problems ", *Technical Report, Texas Institute for Computational and Applied Mathematics(TICAM)*, 1995

[3] Nicolas Moes, John Dolbow and Ted Belytschko, " A Finite Element Crack Growth Method without Remeshing ", *International Journal for Numerical Methods in Engineering*, Vol. 46, 131-150, 1999

[4] M. Fleming, Y. A. Chu and T. Belytschko, " Enriched Element Free Galerkin Method for Crack tip fields ", *International Journal for Numerical Methods in Engineering*, Vol. 40, 1483-1504, 1997

[5] Shafique M. A. Khan and Marwan K. Kharaisheh, " Analysis of Mixed Mode Crack Initiation Angles under Various Loading Conditions ", *Engineering Fracture Mechanics*, **67**, 397-419, 2000.

[6] T. Strouboulis, I. Babuska and K. Copps, " The Design and Analysis of the Generalized Finite Element Method ", *Computer Methods in Applied Mechanics and Engineering*, **181**, 43-69, 2000

[7] The Computational Mechanic Company Inc. (COMCO), " A technical note on Meshless EPM Solver Technology for Structural Mechanics Problems ", *EPM Technical Note*, 1999

[8] The Computational Mechanic Company Inc. (COMCO), " hp - Meshless Method for Dynamic Fracture Propagation ", *EPM Technical Note*, 1999

[9] C. A. Duarte, O. N. Hamzeh, T. J. Liszka and W. W. Tworzydlo, " A Generalized Finite Element Method for the Simulation of three dimensional Dynamic Crack Propagation ", *Computer Methods in Applied Mechanics and Engineering*,**190**, 2227-2262, 2001

[10] S. E. Benzley, " Representation of Singularities with Isoparametric Finite Elements ", *International Journal for Numerical Methods in Engineering*, Vol. 8, 537-547, 1974

[11] T. Belytschko, Y. Y. Lu and G. Lu, " Element Free Galerkin Method ", *International Journal for Numerical Methods in Engineering*, Vol. 37, 229-256, 1994

[12] Barna Szabo and Ivo Babuska, " Finite Element Analysis ", *John Wiley & Sons Inc.*

[13] L. B. Freund, " Dynamic Fracture Mechanics ", *Cambridge University Press*

[14] Kare Hellan, " Introduction to Fracture Mechanics ", *McGraw - Hill Book Company*

[15] P. Kumar, " Elements of Fracture Mechanics ", *Wheeler Publishing*

[16] Robert D. Cook, David S. Malkus and Michael E. Plesha, " Concepts and Applications of Finite Element Analysis ", *John Wiley & Sons Inc.*, Third Edition